Escuela de Ingeniería y Arquitectura
Universidad Zaragoza

MODELING OF HYDROGEL DEFORMATION DUE TO CELL EXERTED FORCES, MIGRATION AND PROLIFERATION

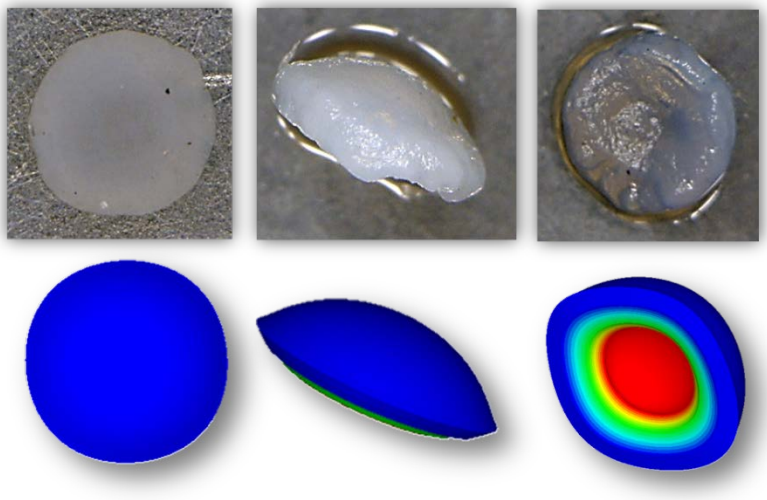

Presented by

Sara Manzano Martínez

Supervised by

Mohamed Hamdy Doweidar

Dr. Mechanical Engineer

Manuel Doblaré Castellano

Dr. Mechanical Engineer

Master in Biomedical Engineering

Postgraduate Program in Transversal Engineering

School of Engineering and Architecture

University of Zaragoza

Zaragoza, September 2011

Me gustaría expresar mi agradecimiento a los Directores de este proyecto, D.Mohamed Hamdy Doweidar y D. Manuel Doblaré Castellano por su paciencia, por su apoyo y especialmente por la ilusión con la que transmiten su conocimiento y experiencia.

A Raquel, Iñaki y Clara por su ayuda y enseñanzas en los numerosos aspectos biológicos presentes en este trabajo. A Berta del ICMA por su dedicación y sus consejos.

A todos mis compañeros, doctores y becarios, por hacerme pasar tan buenos momentos y ayudarme siempre con una sonrisa.

Especialmente, me gustaría agradecer a mi familia, por su apoyo constante y por llenarme el día a día de ánimo y cariño. Dedico a ellos este proyecto y principalmente a mi hermana la Dr. Raquel Manzano, quién me transmite la ilusión por la investigación, es parte fundamental de todos mis trabajos y compañera de batallas.

MODELADO DE LA DEFORMACIÓN DE UN HIDROGEL DEBIDO A LAS FUERZAS CELULARES, MIGRACIÓN Y PROLIFERACIÓN.

RESUMEN

Este proyecto se ha desarrollado en el departamento de Ingeniería Mecánica. El principal objetivo del mismo ha sido la mejora de un modelo computacional de contracción experimentada por un hidrogel debido a las fuerzas ejercidas por las células embebidas. De forma paralela, se han llevado a cabo diferentes experimentos con el fin de lograr una mayor comprensión del proceso y validar el modelo computacional desarrollado. Dicho proyecto se encuentra incluido en una línea de investigación mayor que trata de determinar y cuantificar la influencia de factores mecánicos en el comportamiento celular.

La interacción célula-sustrato es un tema que genera gran interés en la comunidad científica debido principalmente a su conexión con importantes procesos biológicos como la angiogénesis o enfermedades como el cáncer. En esta interacción la célula ejerce una fuerza que será transmitida al sustrato (gel) produciendo la deformación del mismo al objeto de establecer un mecanismo mecano-sensor del microambiente que la rodea.

Existen numerosas evidencias que muestran la gran importancia de de las características mecánicas del entorno circundante en procesos tales como la proliferación, diferenciación y migración celular. Para comprender mejor esta interacción mecanobiológica, y partiendo de un modelo previo de reacción-difusión, se ha generado un modelo que permite simular la deformación que experimenta un gel que contiene fibroblastos en su interior, cuantificar la fuerza celular necesaria para que el proceso tenga lugar y es capaz de predecir la distribución y concentración celular.

Las principales tareas de este proyecto se resumen a continuación. En primer lugar, se han realizado diversos experimentos en el laboratorio para comprender el proceso de contracción del hidrogel, obtener datos experimentales precisos del proceso y determinar la influencia de los diferentes parámetros mecánicos y biológicos. Para ello se han manejado diferentes dispositivos (microscopio optico confocal, lupa de 40X,). Se han incorporado los fenómenos de migración y proliferación al modelo para lograr la deformación observada experimentalmente. Y finalmente, se ha modificado el comportamiento del material (gel) para asemejarlo al observado experimentalmente.

Contents

List of Figures

List of Tables

Chapter 1

Introduction

1.1 Motivation

Cells behavior *in-vitro* is widely studied a 2D environment (Discher, Janmey et al. 2005); however, *in-vivo*, cells live into a complex three-dimensional network, the extracellular matrix (ECM), which not only serves to provide structural and organizational guides for tissue development but also defines and maintains cellular phenotype and drives cell fate decisions. Therefore, to better represent the environment of cells inside the organism and the phenomena that take place, it seems logical to direct researches towards the development of 3D models. Moreover, understanding the interaction between cells and the 3D surrounded environment could be the key for understanding many physiological and pathological situations ranging from embryogenesis to tumor invasion and wound healing (Zaman, Kamm et al. 2005; Manoussaki, Lubkin et al. 1996). In this line, recent evidences suggest that mechanical characteristics of the extracellular matrix, provided vital instructional cues to induce cells to migrate in a certain direction and even stimulate them to proliferate (Even-Ram and Yamada 2005). Mathematical models and computational simulations can provide some insight into these matters. In line with our previous experiences (Manzano, Doweidar et al. 2010), in this work, I present an improved model including essential biological processes as migration and proliferation. The model represents the hydrogel response due to the action of embedded cells and its morphological changes.

1.2 Objectives

The empirical findings describing the contraction of cell substrate hydrogels in the course of the culturing process, prompted us to develop an initial model that enables the study of the cellular and mechanical processes underlying this behavior (Manzano, Doweidar et al. 2010). Although this model has a significant value for the quantification of the biological parameters, the needing of imposing cell concentrations and distribution to obtain the described changes prevents its use for obtaining a simulation of the whole process.

The aim of the present work is the improvement of this previous 3D computational model to simulate cell-generated mechanical forces, substrate deformation, cellular concentration and

morphological changes during the whole process of hydrogel contraction. For this purpose the following specific objectives have been considered:

1. Incorporate essential biological processes, migration and proliferation.
2. Considering consistent hydrogel behavior according to experimental observations. This is to consider collagen fibers reorganization, giving some plasticity to the hydrogel and producing its deformation under cell-exerted forces.
3. Validation of the proposed 3D computational model in collagen hydrogels with embedded cells and determination of its mechanical and biological parameters.

1.3 Description of the project

The presented project is divided into six chapters, ***Chapter 1*** is the introduction while the ***Chapter 2*** contains a general revision of the cell mechanic theory as well as an overview of the cellular contraction process and the main phenomena involved.
Chapter 3 initially describes the previous 3D model on which the present model has been based, establishes the starting hypothesis and steps carried out to the development of this model, and the variations performed to improve the previous model.
Chapter 4 summarizes the biological experiments carried out to quantify the main parameters included in the computational model presented and to characterize the morphological changes observed in the hydrogel.
Chapter 5 analyses the results obtained and the validation of the computational model comparing the experimental results with data obtained from the simulation and its discussion.
Finally, ***Chapter 6*** exposes the main conclusions obtained from this work and future research lines.

Chapter 2

Cell Mechanics

2.1 Introduction

Living organisms show the remarkable ability to change not only their geometry, but also their internal architecture and material properties in response to environmental changes. Mechanics is relevant to several aspects of biology, depending on the specific spatial scale size under consideration: the molecular scale; the cellular scale; the tissue scale (growth and remodeling); and the organ scale (Painter and Sherratt 2003) (Figure 2.1).

This emerging field which study the interface between biology and mechanic is called Mechanobiology. It is mainly focuses on the way that physical forces and changes in cell or tissue mechanics contribute to development, physiology, and disease. While medicine has typically looked for the genetic basis of disease, advances in mechanobiology suggest that changes in cell mechanics, extracellular matrix structure, or mechanotransduction may contribute to the development of many diseases, including atherosclerosis, asthma, osteoporosis, heart failure, and cancer (Holmes and Sleeman 2000).

Nowadays, it is well known that the role of mechanics is even more crucial at a cellular level: why cells are able to deform the substrate where are anchored?; how is cell traction

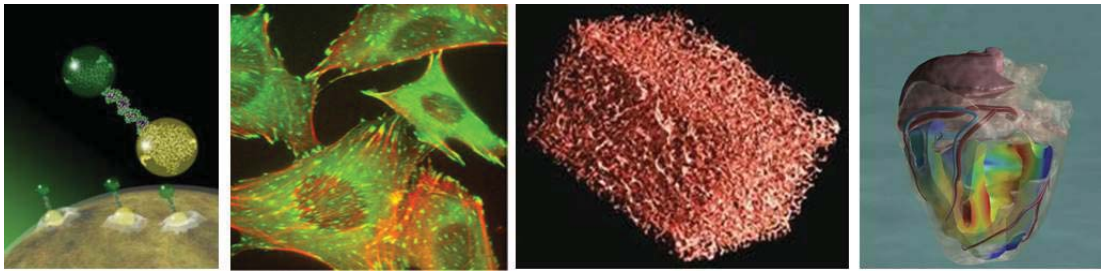

Figure 2.1: *Interaction between mechanic and biology. From left to right, molecular scale: different forces act in DNA transcription process. Cell scale: cell migration take place thanks to forces that anchor cells to the subrtratum called focal adhesions. Tissue scale: cell scaffolds mimic bone marrow. Organ scale: computational model of heart developed by University of Montreal considering main forces (Réseau Québécois de calcul de haute performance (2011)).*

forces transmitted to their surrounding environment; and what are the dynamics governing cell mechanotransduction? These are examples of the basic questions that leading research groups in the world are currently trying to address (Hadjipanayi, Mudera et al. 2009; Rangarajan and Zaman 2008; Ramtani 2004; DiMilla, Barbee et al. 1991). While standard biology answers these questions in a descriptive, empirical manner, mechanics tries to provide a framework for quantitative prediction (DiMilla, Barbee et al. 1991).

2.2 Remarkable cellular phenomena in the hydrogel contraction process

The contraction of collagen hydrogels by fibroblasts has been suggested as a possible in vitro model for connective-tissue reorganization during development (Bell, Ivarsson et al. 1979); granulation tissue contracture during wound healing (Zahm, Kaplan et al. 1997) or some diseases (Tingstrom, Heldin et al. 1992). In addition, the contracted hydrogels have potential clinical importance in the development of artificial skin that could be used in treating major wounds involving loss of substantial amounts of skin such as result from serious burns.

In general, several authors are in agreement with the theory of three key phenomena that lead to hydrogel contraction process observed experimentally: migration, proliferation and traction mechanism produced by the actin-myosin machinery of embedded cells. An essential aspect to point out, and including in this work, is the study of such phenomena acting together, as in the interior of the bodies. Previous to modelation phase, it is necessary to understand each of this phenomena in order to characterize the biological and mechanical parameters that are involved. Below, a short description of them are performed.

2.2.1 Contraction mechanism of hydrogels

Cells contain a network of fibers that provides them support and helps maintain its shape. But even more, this is a dynamic system that interacts with other cellular components to generate a traction and compression mechanism. This structure is called cytoskeleton, and it is mainly composed of three cytoesqueltal filament: microtubules, microfilaments or actin filaments and intermediate filaments (Figure 2.2.b) . These elements conform the actin-myosin machinery mentioned above which is responsible for regulating the force generated by cells (Figure 2.2.a). These forces are transmitted to the ECM through a intermembrane proteins, so called, *integrins,* whose main function is to anchor the cell to the substratum. Finally, transmitted forces produce the physical rearrangement of the collagen fibrils (rather than collagen degradation) within the collagen hydrogels and subsequently morphological changes observed experimentally (Figure 2.2.c). Once the deformation is produced, it is believed that cells adapt to their new surrounding environment and generate a new response (Figure 2.2.d).

2.2.2 Cell migration

Many cells migrate, certainly during development (as various parts of the organism grows), but also at maturity for purposes of wound healing (while cells from the new tissue, it migrate into the wound and renew the tissues) and in combating infection (when cells of the immune system transmigrate from the vascular system across the vessel wall and into the infected tissues). Migration is also an essential feature in cancer metastasis and during angiogenesis, the generation of new vessels. Descriptions of cell migration depict a process that occurs in several stages: protrusion, the extension of the cell at the leading edge in the direction of movement; adhesion of the protrusion to the surrounding substrate or matrix; contraction of the cell that transmits a force from these protrusions at the leading edge to the cell body, pulling it forward; and release of the attachments at the rear, allowing net forward movement of the cell to occur (Hadjipanayi, Mudera et al. 2009; DiMilla, Barbee et al. 1991). While it is well known that cells sense biochemical cues such as gradients in chemotactic agents, they can also apparently sense their physical environment, because their direction of migration can be influenced by variations in the stiffness of the substrate to which they adhere. Whatever the mode of migration, however, the central role of cell mechanics, both passive stiffness and active contractility, is clear.

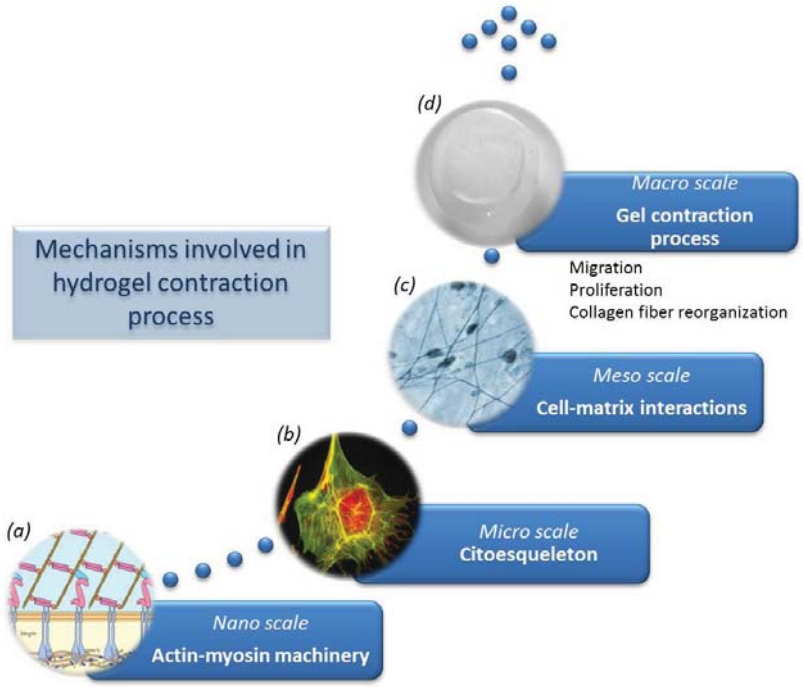

Figure 2.2: *Main mechanism involved in the process of hydrogel contraction. (a)Actin-myosin machinery acts in order to produce cell forces as response of mechanical and chemical signals. (b) Cytoesqueleton are composed of filaments whose main function . (c) Cells interact with their surrounded environment by transmiting forces and producing the reorganization of the collagen fibers. (d) This reorganization ended into new structures and cell exerted forces generate a typical hydrogel deformation.*

2.2.3 Cell proliferation

Cell proliferation is the increase in cell number as a result of cell growth and division. The accurate assessment of cell number and cell proliferation is useful in many high content assays and is a key readout in cytotoxicity and apoptosis applications. Cell proliferation is also a very sensitive indicator of cell stress since it requires intact cell structures and function.

Chapter 3

3D Model of Hydrogel Contraction Including Cell Migration and Proliferation

In this chapter, firstly, it shall gives a brief description of our previous model (Manzano, Doweidar et al. 2010) based in the theory proposed by Murray, Oster and Harris (Murray, Oster et al. 1983), emphasizing in the lacks observed. Secondly, different solutions and modelation of experimental phenomena are proposed. Finally, a mathematical formulation of the problem was developed in order to obtain the set of non-linear equation required to the Finite Element analysis.

3.1 Previous mechanobiological models of hydrogel contraction

The literature shows different models related vasculogeneis or angiogenesis, where cell substrate interaction is of particular interest (Murray 2003). However, when the aspect to consider is the study of morphological changes undergone by the substrate due to the cells seeded inside, this turns out complicated.

Our previous 3D model of hydrogel contraction is based in the theory presented by Oster, Murray and Harris for the study of mechanical aspects in mesenchymal morphogenesis (Oster, Murray et al. 1983) and, it is an extension of the 2D mechanosensing model describing by Moreo and cols., as also consider the mechanical interactions between cells and extracellular matrix (Moreo, Garcia-Aznar et al. 2008). This previous model presents a valuable tool when knowing the cellular distribution that generates the experimental hydrogels shapes. Therefore it is capable to quantify essential parameters like cell forces and provide some insight in the study of the influence of rigidity and viscosity in the behavoiur of the hydrogel.

However, after further study of cell behavior and the response produced in the hydrogel,

there are significant limitations to this model to reproduce the experimental process. The main shortcomings of the previous model are those summarized below.

1. The needing of imposing cell concentrations and distribution to obtain the desired changes, prevents its use for obtaining a complete simulation of the whole process.

2. Essential processes such as migrations and proliferation are missed. Both factors are necessary in completing the morphological changes experienced by the hydrogel.

3. Finally, experiments show how cells are able to reorganize collagen fibers by creating new structures as a response of cell-exerted forces. Therefore, this observation must be reflected in the behavior of the hydrogel.

3.2 Proposed improvements

The following improvements were proposed in order to obtain a more realistic model capable of reproducing the morphological changes observed in our experiments.

3.2.1 Modeling the behavior of the hydrogel as a visco-elastoplastic material which deforms under cell-exerted forces

In 1985, Gridry and Grinnell were the first to highlight the reorganization of collagen fibers due to fibroblasts deposited on the top of the gel (Guidry and Grinnell 1985). They showed how sparse, randomly and packed collagen fibrils originally found in gels become densely packed and aligned during gel reorganization. They also appreciated that only 5% of the collagen was degraded, although the volume of the gels decreased by 85% or more. It could be concluded, therefore, that gel reorganization required physical rearrangement of pre-existing collagen fibrils rather than degradation of the original collagen or synthesis of new matrix. This will be essential in order to establish the main hypothesis of our computational model.

On the other hand, even today it is unclear why this reorganization of collagen occurs, and in absence of experimental evidences that confirm this behavior when cells are seeding inside, the vast majority of mechanobiological models, as well as our previous model, assumed the behavior of the substratum as a viscoelastic material.

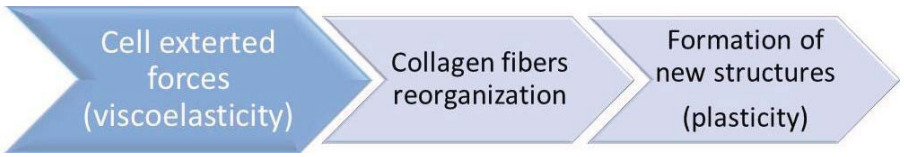

Figure 3.1: *Relationship of cell exerted forces and hydrogel response by formating new stable structures.*

However, according with our last experimental research, even when removing cells inside the hydrogel, it keeps its shape and geometry. Exceptionally, a small quantity of collagen was unstable and could not hold its position without continued force exerted by the cells. This led us

to think about vico-elastoplastic hydrogel behavior able to capture, first of all, the viscoelastic behavior in the early phase of application of cell forces and, secondly, the plasticity could be considered in the reorganization of collagen fibers phase as it is shown in Figure 3.1.

3.2.2 Modeling cell migration and proliferation

Cell proliferation is necessary to complete the morphogenetic changes. Experimental results indicates that, during the morphological event, the cell density increases not only because of contraction, but also because of proliferation, suggesting that the system needs to reach a critical number of cells for this phenomenon to occur (Quintana, Muinos et al. 2009). Hence, the modelation of cell proliferation is necessary to obtain the final shape observed experimentally. Apart from this, a minimum number of cells is necessary (cell concentration equal to or greater than 2000 cells per cm^3) in order to start the contraction process (Quintana, Muinos et al. 2009). To model this phenomenon it is adopted the Malthus theory (Murray 2003) described below.

As for cell migration, similarly to living organism, cells can move from one point to another. To model this phenomena, it is necessary to considered two important processes,

- The first, it is due to diffusive processes, which tend to disperse cells in the hydrogel and cause a homogeneous spatial distribution.

- And the second ones related to several effects which tends to organize cell population by allowing cells to move into regions where the cell density is already higher than the surrounding area (aggregation phenomena).

Diffusion has already been considered in the previous model (Manzano, Doweidar et al. 2010). Hence, in the following section we will focus on explaining these "anti-diffusion" phenomena not included initially: convective motion and haptotaxis.

Summarizing, our basic assumption is that migration is the primary event and it plays a leading role in morphological changes, while proliferation is secondary but provides the necessary cell concentration to produce the force which will complete the contraction process.

3.2.3 Adjustment of the mechanical and biological parameters.

Experimental data included in the literature shown an enormous variability (Guidry and Grinnell 1985; Ferrenq, Tranqui et al. 1997). Although there is agreement in the morphological changes observed, it exists a wide range of values for hydrogel diameter. In order to quantify mechanical parameters of the substrate, different experiments were performed. This part is highly developed in ***Chapter 4:*** Experimental Work. Besides, the application of this parameters to the computational model gave the morphology observed experimentally (see ***Chapter 5*** of Numerical Validation, results and discussion).

3.3 Mathematical formulation of the problem

The mechanocelullar framework proposed by Murray, Oster and Harris to describe cell dynamics, cell-ECM interactions and the resulting state of strain in the ECM has been used for analyzing the spatio-temporal organization of tissue in various biological contexts (Murray, Oster et al. 1983). More specifically, such models can describe the cell-induced contraction of the ECM.

As some mechano-biological models (DiMilla, Barbee et al. 1991), two main species have been considered in this model, cells and ECM, being characterized by cellular concentration (c) and ECM density (ρ) respectively. A continuum approach has been adopted, considering the fundamental conservation law for the concentration of each species.

3.3.1 Law of conservation of species $Q(x,t)$

The local changes in cell concentration and ECM density following the conservation law of species can be expressed as (Ferrenq, Tranqu et al. 1997):

$$\frac{\partial Q}{\partial t} = -\nabla \mathbf{J}_Q + f_Q \tag{3.1}$$

where $\mathbf{J}_Q$ denotes the flux of each specie Q and f_Q is the rate of production of Q.

3.3.2 ECM density $\rho(x,t)$

During the development, in vivo, cells generate, and degrade collagen ECM (Ghosh, Pan et al., 2007). By contrast, in vitro, these processes are inhibited, leading to consider the rate of ECM production as null (Guidry and Grinnell 1985), then $f_\rho = 0$. Thus, the local changes in extracellular matrix are only influenced by the cells migration from one point to other in the gel, which is known as passive convection and can be defined as,

$$\mathbf{J}_\rho = \rho \frac{\partial \mathbf{u}}{\partial t} \tag{3.2}$$

where $\mathbf{u}$ denotes the displacement vector of each point of the ECM.

3.3.3 Cellular Concentration $c(x,t)$

In cellular flux $\mathbf{J}_c$, indicates the movement of cells, and as it was discussed in the previous section, two important phenomena take place,

a) Diffusion phenomena

Random, non-directed cell movement is analogous to diffusion of particles in a gas o liquid, and the same mathematical treatment can be used to described both situations. Random motions are conventionally modeled as a diffusion process where Fick´s Law governing diffusion molecules. It is denoted by $\mathbf{J}_{diff}$, the flux of cells passing through one cm^3 of hydrogel. Fick´s law states that this flux is proportional to the gradient in cell concentration ∇c . Then,

$$\mathbf{J}_{diff} = -D\nabla c \tag{3.3}$$

where D is the diffusion coefficient.

b) Aggregation phenomena related to traction forces of the cells: passive convection and haptotaxis.

Opposite to these dispersive forces which tend to create a homogeneous spatial distribution of cells, exists several effects which tend to organize cell population by migration of cells from one area to another with a higher cell concentration. In fact, these effects can be deduced from known phenomena of cells behavior in tissue culture.

- *Passive convection* ($\mathbf{J}_{conv}$)*: cells can be passively dragged*

Cells can be passively dragged along by the contractions of its immediate neighbours, or on the substratum which is being dragged by the contractions of distant cells. For cells in vivo, the substratum is the extracellular matrix and/or other cells. The expression for convective cell motions has the form,

$$\mathbf{J}_{conv} = \rho \frac{\partial \mathbf{u}}{\partial t} \tag{3.4}$$

being $\frac{\partial \mathbf{u}}{\partial t}$ the mean cell velocity, that is the local mean velocity of the matrix the cells are sitting on.

- *Haptotaxis: cells will follow an adhesive gradient.*

Motile cells will move from less adhesive to more adhesive regions of their substrata (Hawkins, Piel et al. 2009). The directionality of this movement results from competition between opposite sides of individual motile cells: each side of a cell forms adhesions in the substratum and engages in a tug-of-war with net displacement occurring in direction of that side with the strongest pull and the firmest attachments to the substratum. Thus a cell's otherwise random motion will be biased up the adhesive gradient. We can model this effect by writing the cell flux due to haptotaxis as,

$$\mathbf{J}_{hapt} = [c][average\ cell\ velocity\ up\ the\ gradient] \tag{3.5}$$

The simplest way to relate the net cell velocity up the adhesive gradient to the steepness of the gradient is to assume that the mean velocity of migration is proportional to the steepness of the gradient. That is,

$$\mathbf{J}_{hapt} \sim [c][gradient\ in\ adhesiveness] \tag{3.6}$$

The local density of adhesive sites is proportional to the density of the matrix material. Therefore, we can write the above equation as,

$$\mathbf{J}_{hapt} = h[c][\nabla \rho_{ECM}] \tag{3.7}$$

where the parameter h is the 'haptotactic coefficient', which measures a cell's tendency to move up an adhesive gradient - analogous to the diffusion coefficient, which measures the tendency of a cell to move down a cell-density gradient.

Both equations, gives the total cellular flux:

$$\mathbf{J}_c = \mathbf{J}_{diff} + \mathbf{J}_{conv} + \mathbf{J}_{hapt} \tag{3.8}$$

$$\mathbf{J}_c = -D\nabla c + c\frac{\partial \mathbf{u}}{\partial t} + hc\nabla\rho_{ECM} \tag{3.9}$$

For modeling the proliferation (f_c), it is considered the Malthus theory (Murray 2003). This considered $N(t)$ as the population of the species at time t, then the rate of change is

$$\frac{dN}{dt} = births - deaths \tag{3.10}$$

this simple equation represents a conservation equation for the cell population. The form of the various terms on the right hand side of (3.10) necessitates modeling the situation with which we are concerned. The *birth* and *death* terms are proportional to N. That is,

$$\frac{dN}{dt} = bN - dN \Longrightarrow \frac{dN}{dt} = (b-d)N = rN \tag{3.11}$$

where b, d are positive constants and the initial population $N(0) = N_o$. Thus if $b > d$ the population grows exponentially while if $b < d$ it dies out.

3.3.4 ECM displacement $\mathbf{u}(x,t)$

To calculate the displacement of each point of the extracellular matrix, there is the balance of linear momentum. Being $\boldsymbol{\sigma}_{ecm}$, the ECM stress that depends on the ECM displacements $\mathbf{u}$; and $\mathbf{f}_{ext}$ the external forces. The mentioned balance can be exposed as the following,

$$\nabla(\boldsymbol{\sigma}_{cell} + \boldsymbol{\sigma}_{ecm}) + \mathbf{f}_{ext} = 0 \tag{3.12}$$

Being $\mathbf{f}_{ext}$ the external forces and $\boldsymbol{\sigma}_{ecm}$, the stress of cell population. As other mechanobiological model (Murray, Oster et al. 1983), it is considered to be proportional to the tension exerted by a single cell (p_{cell}) and cellular concentration (c). Can be expressed as follows,

$$\sigma_{cell} = \frac{p_{cell}}{1+\lambda c} cI \tag{3.13}$$

being λ a parameter which characterizes the saturation of the cell stress and I is the identity second order tensor.

3.3.5 Summary of the main equations

Substituting the previous equations 3.4, 3.9 and 3.12 in the conservation law (equation 3.1) yields the following set of partial deferential equations:

$$\frac{\partial c}{\partial t} + \nabla[-D\nabla c + c\frac{\partial \mathbf{u}}{\partial t} + h\nabla\rho_{ECM}] = rc$$

$$\frac{\partial \rho}{\partial t} + \nabla[\rho \frac{\partial \mathbf{u}}{\partial t}] = 0$$
$$\nabla(\boldsymbol{\sigma}_{cell} + \boldsymbol{\sigma}_{ecm}) + \rho \mathbf{f}_{ext} = 0 \tag{3.14}$$

For a general linear viscoelastic behavior assumed for the ECM, the following formula is proposed (Ramtani, 2004):

$$\sigma_{ecm} = \frac{E}{1+\nu}[\boldsymbol{\varepsilon} + \frac{\nu}{1-2\nu}\theta \mathbf{I}] + \mu_1 \frac{\partial \boldsymbol{\varepsilon}}{\partial t} + \mu_2 \frac{\partial \theta}{\partial t}\mathbf{I} \tag{3.15}$$

being $\boldsymbol{\varepsilon}$ the ECM strain tensor under the small strains assumption, $\mathbf{I}$ the second order identity tensor , E and ν the Young modulus and Poisson ratio of the ECM and μ_1 and μ_2 its shear and bulk viscosity, respectively.

For the reorganization of collagen fiber (described in detail in section 3.2), periodic downloads of the internal stresses of the hydrogel carry out in order to simulate the consolidation of new networks of collagen that occur once the forces exerted by the cells are balanced with the resistance opposed by the hydrogel.

3.4 Initial and boundary conditions

Considering generic initial conditions for the cell concentration and substrate density, $c(x,0) = c_o(x,t)$ and $\rho(x,0) = \rho_o(x,t)$, the weak formulation is obtained. Moreover, initially an undeformed state is assumed, so $\mathbf{u}(x,0) = \mathbf{0}$. Furthermore, the hypothesis of small strains and displazaments is assumed in this model.

As boundary conditions, zero flux was considered for each species (cellular concentration, c , and density of the ECM, ρ) on the contour $\partial\Omega$ of he domain Ω. Furthermore, it is assumed that the displacements in x and y axes, u_x and u_y equal to zero in a central point located in the bottom area of the substrate just to avoid its translation, as well as u_z equal to zero in the peripheral contour of the bottom of the hydrogel, as shown in Figure 3.2.a.

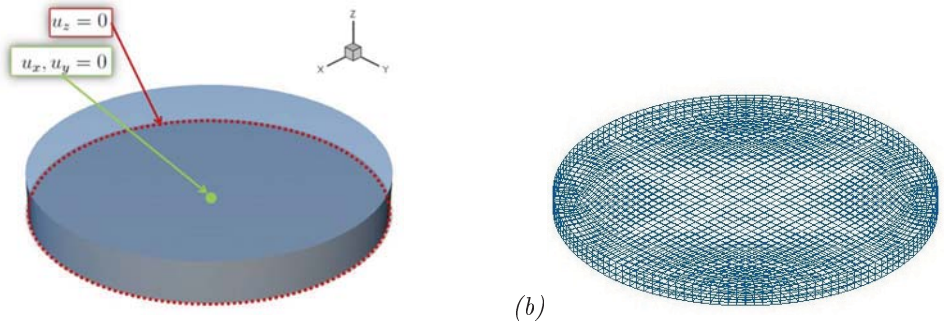

(a) *(b)*

Figura 3.2: *(a) Boundary conditions of the hydroegl. (b) Mesh of the hydrogel with 8-node hexaedron elements.*

3.5 Numerical solution

A finite element analysis is adopted for the solution of the governing system of equations. The primary unknowns of the model are interpolated from nodal values through shape functions as usual, and the time derivatives are approximated with a generalized trapezoidal method.

3.5.1 Weak formulation

In order to obtain the fully coupled nonlinear system of equations describing the discretized model, we first reproduce the weak formulation of the governing equations. As usual, with nonlinear conservation laws, there are no smooth solutions to this equation and we have to consider weak solutions, as follow,

$$\int_\Omega \delta c \frac{\partial c}{\partial t} dV + \int_\Omega \nabla \delta c [D\nabla c - c\frac{\partial \mathbf{u}}{\partial t} - hc\nabla\rho] dV = \int_\Omega \delta c r c dV$$

$$\int_\Omega \delta\rho \frac{\partial \rho}{\partial t} - \int_\Omega \nabla\delta\rho \frac{\partial \mathbf{u}}{\partial t} dV = 0$$

$$\int_\Omega \frac{1}{2}(\nabla\delta\mathbf{u} + \nabla^T\delta\mathbf{u}) dV - \int_\Omega f_{ext} dV = 0 \tag{3.16}$$

3.5.2 Discretization and non-linear equations system

Temporal discretization of the problem

For the temporal discretization of the set of governing equations, let us consider a partition $\cup_{n=1}^{n_{step}-1}[t_n, t_{n+1}]$ of the time interval of interest T, and focus on the typical time subinterval $[t_n, t_{n+1}]$ with $\triangle t = t_{n+1} - t_n \geq 0$ denoting the corresponding increment of time. It is assumed that the primary unknowns and all derivable quantities are known at time t_n. It is applied the generalized trapezoidal method (Hughes 1987) defined by $\alpha \epsilon (0, 1]$, such that $t_{n+\alpha} = t_n + \alpha\Delta t$. In this method the following scheme is used for the temporal discretization of primary variables (only shown for c, being identical for ρ and u):

$$c_{n+1} = c_n + \triangle t \dot{c}_{n+\alpha} \tag{3.17}$$

$$\dot{c}_{n+\alpha} = c_n(1-\alpha) + c_{n+1}\alpha \tag{3.18}$$

where c_{n+1}, $\dot{c}_{n+\alpha}$ y $\dot{c}_{n+1}$ are approximations of $c(t_{n+1})$, $(\partial c/\partial t)(t_{n+\alpha})$ and $(\partial c/\partial t)(t_{n+1})$, respectively. From a practical standpoint it is introduced $\tilde{c}_{n+1}$ as a predictor value of c_{n+1}, which only depends on magnitudes at time t_n:

$$\tilde{c}_{n+1} = c_n + (1-\alpha)\triangle t \dot{c}_n \tag{3.19}$$

and compute $\dot{c}_{n+1}$ simply as

$$\dot{c}_{n+1} = \frac{c_{n+1} - \tilde{c}_{n+1}}{\alpha \triangle t} \tag{3.20}$$

Substitution of 3.19 and 3.20 in the weak form of the problem given by equation 3.16 yields a semi-discrete set of equations discretized in time.

Spatial discretization of the problem

Next, the semi-discrete system is discretized in space making use of the finite element method. Classically, in the spirit of the finite element method, the underlying domainΩ is discretized into n_{el} elements Ω^e, with $\Omega = \cup_{e=1}^{n_{el}} \Omega^e$. The primary unknown fields are interpolated within a generic element Ω^e in terms of the nodal values through shape functions, that is,

$$c^h \mid_{\Omega^e} = N_c c^e$$

$$\rho^h \mid_{\Omega^e} = N_\rho \rho^e$$

$$u^h \mid_{\Omega^e} = N_u u^e \tag{3.21}$$

where c^e ,ρ^e y u^e are column vectors of nodal values of the primary unknowns at element e and N_c, N_ρ and N_u are matrices of element shape functions, that is,

$$N_c = [N_c^1, \ldots, N_c^{n_{en}}]$$

$$N_\rho = [N_\rho^1, \ldots, N_\rho^{n_{en}}]$$

$$N_u = \begin{bmatrix} N_u^1 & 0 & 0 \\ 0 & N_u^1 & 0 \\ 0 & 0 & N_u^1 \end{bmatrix} \cdots \begin{bmatrix} N_u^{n_{en}} & 0 & 0 \\ 0 & N_u^{n_{en}} & 0 \\ 0 & 0 & N_u^{n_{en}} \end{bmatrix} \tag{3.22}$$

with N^i the shape function associated to element node i and n_{en} the number of element nodes. Following a Bubnov-Galerkin scheme, the same shape functions are also applied to interpolate the test functions:

$$\delta c^h \mid_{\Omega^e} = N_c \delta c^e$$

$$\delta \rho^h \mid_{\Omega^e} = N_\rho \delta c^e$$

$$\delta u^h \mid_{\Omega^e} = N_u \delta u^e \tag{3.23}$$

Likewise, the discretization of the related gradients of the test functions and the primary unknowns take the following element wise format:

$$\nabla c^h \mid_{\Omega^e} = \nabla N_c c^e \Longrightarrow \nabla \delta c^h \mid_{\Omega^e} = \nabla N_c \delta c^e$$

$$\nabla \rho^h \mid_{\Omega^e} = \nabla N_\rho \rho^e \Longrightarrow \nabla \delta \rho^h \mid_{\Omega^e} = \nabla N_c \delta \rho^e \tag{3.24}$$

Finally, the strains are interpolated in the following form:

$$\varepsilon^h \mid_{\Omega^e} = B_u u^e \tag{3.25}$$

being B_u is a matrix of derivatives of shape functions:

$$B_u = H N_u$$

$$H = \begin{bmatrix} \frac{\partial}{\partial x} & 0 & 0 \\ 0 & \frac{\partial}{\partial x} & 0 \\ 0 & 0 & \frac{\partial}{\partial x} \\ \frac{1}{2}\frac{\partial}{\partial y} & \frac{1}{2}\frac{\partial}{\partial x} & 0 \\ \frac{1}{2}\frac{\partial}{\partial y} & 0 & \frac{1}{2}\frac{\partial}{\partial x} \\ 0 & \frac{1}{2}\frac{\partial}{\partial z} & \frac{1}{2}\frac{\partial}{\partial y} \end{bmatrix} \tag{3.26}$$

Substituting the equations 3.21, 3.23 and 3.25 into the semi-discrete system and choosing appropiately the arbitrary coefficients δc^e, $\delta \rho^e$y $\delta u^e$of the test functions, one can finally arrive to a set of non-linear algebraic equations which is sufficient to determine the nodal values of the primary unknowns and can be written in the form:

$$\mathcal{F}^{int}(\mathbb{Z}_{n+1}, \frac{\mathbb{Z}_{n+1} - \widetilde{\mathbb{Z}}_{n+1}}{\alpha \triangle t}) = \mathcal{F}^{ext}(\mathbb{Z}_{n+1}) \tag{3.27}$$

being $\mathbb{Z}_{n+1}$ and $\widetilde{\mathbb{Z}}_{n+1}$ the global column vector of nodal values of the primary unknown fields at time t_{n+1} and the corresponding predictor value, respectively. This vector are obtained as follow:

$$\mathbb{Z}_{n+1} = A_{e=1}^{n_{en}} d_{n+1}^e \tag{3.28}$$

$$\widetilde{\mathbb{Z}}_{n+1} = A_{e=1}^{n_{en}} \tilde{d}_{n+1}^e \tag{3.29}$$

Herein A denotes the standard, finite element, assembly operator and d_{n+1}^e and $\tilde{d}_{n+1}^e$ the column vector with the expressions:

$$d^e_{n+1} = [c^e_{n+1}, \rho^e_{n+1}, u^e_{n+1}]^T$$

$$\tilde{d}^e_{n+1} = [\tilde{c}^e_{n+1}, \tilde{\rho}^e_{n+1}, \tilde{u}^e_{n+1}]^T \tag{3.30}$$

The internal and external global force vector represented by $\mathcal{F}^{int}_{n+1}$ and $\mathcal{F}^{ext}_{n+1}$ also come from the assembly of element contributions:

$$\mathcal{F}^{int}_{n+1} = A^{n_{en}}_{e=1} f^{int,e}_{n+1} \tag{3.31}$$

$$\mathcal{F}^{ext}_{n+1} = A^{n_{en}}_{e=1} f^{ext,e}_{n+1} \tag{3.32}$$

being

$$f^{int,e}_{n+1} = [f^{int,e}_{c,n+1}, f^{int,e}_{\rho,n+1}, f^{int,e}_{u,n+1}]^T \tag{3.33}$$

$$f^{ext,e}_{n+1} = [f^{ext,e}_{c,n+1}, f^{ext,e}_{\rho,n+1}, f^{ext,e}_{u,n+1}]^T \tag{3.34}$$

The element contributions to the internal force read as:

$$f^{int,e}_{c,n+1} = \int N^T_c \frac{c^h_{n+1} - \tilde{c}^h_{n+1}}{\alpha \triangle t} dV + \int \nabla N^T_c [D \nabla c^h - c^h \frac{c^h_{n+1} - \tilde{c}^h_{n+1}}{\alpha \triangle t} - h \nabla \rho^h -$$

$$]_{n+1} dV$$

$$f^{int,e}_{\rho,n+1} = \int N^T_\rho \frac{\rho^h_{n+1} - \tilde{\rho}^h_{n+1}}{\alpha \triangle t} dV + \int \nabla N^T_\rho \rho^h_{n+1} \frac{u^h_{n+1} - \tilde{u}^h_{n+1}}{\alpha \triangle t} dV$$

$$f^{int,e}_{u,n+1} = \int B^T_u [D_{elas} H u^h + D_{visc} H \frac{u^h_{n+1} - \tilde{u}^h_{n+1}}{\alpha \triangle t} + \frac{p_{cell} c^h}{1 + \lambda c^h} I]_{n+1} dV \tag{3.35}$$

where D_{elas} and D_{visc} are the mechanical behavior matrices:

$$D_{elas} = \begin{bmatrix} 1-\nu & \nu & \nu & & & \\ \nu & 1-\nu & \nu & & \tilde{0} & \\ \nu & \nu & 1-\nu & & & \\ & & & 1-2\nu & 0 & 0 \\ & \tilde{0} & & 0 & 1-2\nu & 0 \\ & & & 0 & 0 & 1-2\nu \end{bmatrix} \tag{3.36}$$

$$D_{visc} = \begin{bmatrix} \mu_1+\mu_2 & \mu_2 & \mu_2 & & & \\ \mu_2 & \mu_1+\mu_2 & \mu_2 & & \tilde{0} & \\ \mu_2 & \mu_2 & \mu_1+\mu_2 & & & \\ & & & \mu_1 & 0 & 0 \\ & \tilde{0} & & 0 & \mu_1 & 0 \\ & & & 0 & 0 & \mu_1 \end{bmatrix} \tag{3.37}$$

In the case of the external force vector the element contributions have the following expressions:

$$f^{ext,e}_{c,n+1} = \int N_c^T r c^h_{n+1} dV$$

$$f^{ext,e}_{\rho,n+1} = 0$$

$$f^{ext,e}_{u,n+1} = \int N_u^T \rho^h_{n+1} f_{ext,n+1} dV \tag{3.38}$$

Linearization of the problem

The solution of the set equation system 3.14 is obtained by a standard Newton-Raphson iterative solution procedure. Thereafter, a differentiation between stiffness matrices and mass is done and thus,

$$k^{int,e}_{cc,n+1} = \frac{1}{\alpha \triangle t} \int N_c^T N_c dV + \int \nabla N_c^T D \nabla N_c dV - \int \nabla N_c^T \frac{u^h_{n+1} - \tilde{u}^h_{n+1}}{\alpha \triangle t} N_c dV$$

$$k^{int,e}_{cu,n+1} = -\frac{1}{\alpha \triangle t} \int \nabla N_c^T c^h_{n+1} N_u dV$$

$$k^{int,e}_{\rho\rho,n+1} = -\frac{1}{\alpha \triangle t} \int N_\rho^T N_\rho dV - \int \nabla N_\rho^T \frac{u^h_{n+1} - \tilde{u}^h_{n+1}}{\alpha \triangle t} N_\rho dV$$

$$k^{int,e}_{uu,n+1} = \int B_u^T D_{elas} B_u dV + \frac{1}{\alpha \triangle t} \int B_u^T D_{visc} B_u dV + \int B_u^T \frac{K_{cell} c^h_{n+1}}{1 + \lambda c^h_{n+1}} I \nabla^\dagger N_u dV$$

$$k^{int,e}_{uc,n+1} = \int B_u^T \frac{p_{cell}}{1 + \lambda c^h_{n+1}} I N_c dV$$

$$k^{ext,e}_{cc,n+1} = \int N_u^T r N_c dV$$

$$k^{ext,e}_{uu,n+1} = -\int N_u^T \rho^h_{n+1} N_u dV$$

$$k^{ext,e}_{u\rho,n+1} = -\int N_u^T u N_\rho dV \tag{3.39}$$

For Finite Element analysis, the 8-node hexahedron elements and two Gauss integration points in each direction, are used. The resulting mesh is shown in Figure 3.2.b. The selected mesh size in x, y and z axes is about $2\mu m$, and the total number of elements is 3528. Under these conditions, we observe a fairly good agreement in the solutions that appear with the model and the experimental results. The finite element analysis is realized with the commercial software package ABAQUS 6.8 (www.abaqusdoc.ca/v6.8).

Chapter 4

Experimental Work

Collagen is a fibrous protein that consists of three chains that can combine to form a rope-like triple helix, providing tensile strength to the extracellular matrix (ECM). Type I is the most common fibrillar collagen (90%), and is mainly found in skin, bone, tendons, and other connective tissues. Collagen hydrogel fibrils mimic the solid structure where adherent cells anchor in vivo (ECM) and the study of hydrogel contraction process by embedded cells, could represent a valuable approach to many biological processes such as morphogenesis, vasculogenesis or tumor invasion.

4.1 Background

Several studies reported by Quintana et al. focus on the in-vitro recreation of the biological, biophysical and biomechanical conditions occurring in the development of a tissue structure (Quintana, Muinos et al. 2009). They observed a hydrogel contraction due to fibroblast embedded. Moreover, cell proliferation and migration ended into a range of hydrogel morphological changes (Figure 4.1).

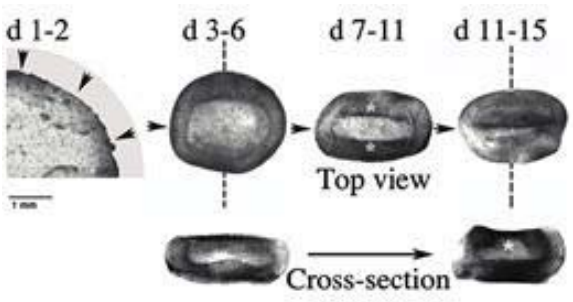

Figure 4.1: *Main morphological process observed using visual inspection of mouse fibroblast cultured with FM in RAD16-I 0.25% (*Quintana, Muinos et al. 2009*).*

In light of these results, Quintana and colleagues proposed that specific cellular distributions consequence of the above mentioned processes of proliferation and migration may lead to the

hydrogel geometric shapes observed experimentally (Quintana, Muinos et al. 2009).

Our previous model of hydrogel contraction (see section 3.1) corroborated these experimental observations. Moreover it is capable of quantifying forces generated by cells during the whole process, as well as the viscosity and stiffness of the hydrogel (Manzano, Doweidar et al. 2010).

4.2 Material and methods

In order to model the hydrogel contraction process, it is necessary to obtain an accurate and reliable measurements of three essential hydrogel parameters: stiffness, diameter variation and morphological changes.

To this aim, a new experimental approach was designed. It consists basically of three phases: the preparation of collagen hydrogels, addition of human fibroblast and monitoring of hydrogel diameter and morphology with optical microscopy. These phases will be described in detail below.

All procedures in this study followed the guidelines of the University of Zaragoza for the human biological sample manipulation. Fibroblasts used in these experiments were obtained from adipose tissue of healthy donors and gently provided by the Biochemistry department of the University of Zaragoza. After 7 days of expansion at standard density with medium , cells were detached by trypsinization.

4.2.1 *Preparation of substrate and incubation of cells with collagen lattices*

Hydrated collagen lattices (0.2 % *w/v*, case A and 0.3 % *w/v*, case B) were prepared by diluting collagen I, Rat Tail and essential medium. Subsequently, $2{\cdot}10^3$ *cells* (case A) and $1{\cdot}10^3$ *cells* (case B) were uniformly mixed with the respective collagen preparations and neutralized with NaOH. 90 (case A) and 120 microliters (Case B) of cell/collagen suspensions were poured over bottom cut eppendorfs and included into petri dishes containing minimal essential medium. Finally, mixtures gelled at 37 °C overnight in the incubator. Hydrogel dimensions were approximately 6 *mm* diameter and 3.2 mm thick (Case A) and 9 *mm* diameter and 2 *mm* thick (Case B).

4.2.2 *Cell culture and hydrogel parameter measurement*

Case A

In this case, the effect of cells death on hydrogel parameters was assessed. After 8 days of culture, cells were killed. Then, measurement of the hydrogel diameter after 72h and 5 days respectively were obtained by confocal microscope.

Case B

The purpose of this experiment was to determine the effects of living cells into the hydrogel morphology and dimensions. In this case, cells were left to proliferate and migrate for 21 days

monitoring. A set of 10 hydrogel fibroblast cultures were established in parallel for statistical analysis of the results.

4.3 Experimental results

In this section, different parameters selected for each experiment are collected, as well as the results obtained.

4.3.1 Sequence of morphological changes and parameter measurement

4.3.1.1 Case A. Hydrogel deformation after killing embedded cells

Hydrogel properties

As above mentioned, the collagen matrix hydrogel prepared in this case presented a 6 mm diameter and 3,2 mm thickness size, a cell concentration of $2,0{\cdot}10^3 cells/mm^3$ and $0,2\%\ w/v$. Detailed information of the parameters measured in this hydrogel is supplied in table 4.1.

Parameter	Description	Value	Units
n_o	Initial fibroblast concentration in the hydrogel	$2.0{\cdot}10^3$	$cells/mm^3$
Ø	Initial diameter of the hydrogel	6.0	mm
e	Initial thickness of the hydrogel	3.2	mm
ρ_{ECM}	Collagen concentration in the ECM	0.002	mg/mm^3
K	Stiffness moduli of the collagen hydrogel	$77.26{\cdot}10^{-6}$	MPa
v	Viscosity of the hydrogel	0.3	

Table 4.1: *Main experimental parameters selected to the collagen hydrogel contraction process.*

Sequence of hydrogel contraction obtained

The main purpose of this experiment was to verify the hypothesis of hydrogel behavior mentioned in section 3.2. It relies on the consideration of the hydrogel as a visco-elastoplastic material where collagen fibrils interact to create 3D structures that counteract the cellular force and impede hydrogel deformation, making necessary an increment in the cellular concentration to overcome this structure and continue the substrate contraction. Therefore, one can speculate that the removal or death of the embedded cells would not induce hydrogel to recover the initial dimensions.

After 8 days of proliferation, cells were killed and the diameter was measure after 72h and 5 days of phosphate buffered saline medium (PBS) incubation respectively. Hydrogel diameter was progressively reduced before cell death (Table 4.2.c). However, the no existence of cells prevented the hydrogel to continue contracting, and no significant differences were observed in the diameter of the substrate after day 11 or 13 respectively (Figure 4.2).

It is important to note the high reduction of the hydrogel diameter (over 30%)(Figure 4.2.a and 4.2.b), during the first three hours of incubation. This phenomenon has been previously described during the polymerization of collagen and is independent of the cell content (Grinnell

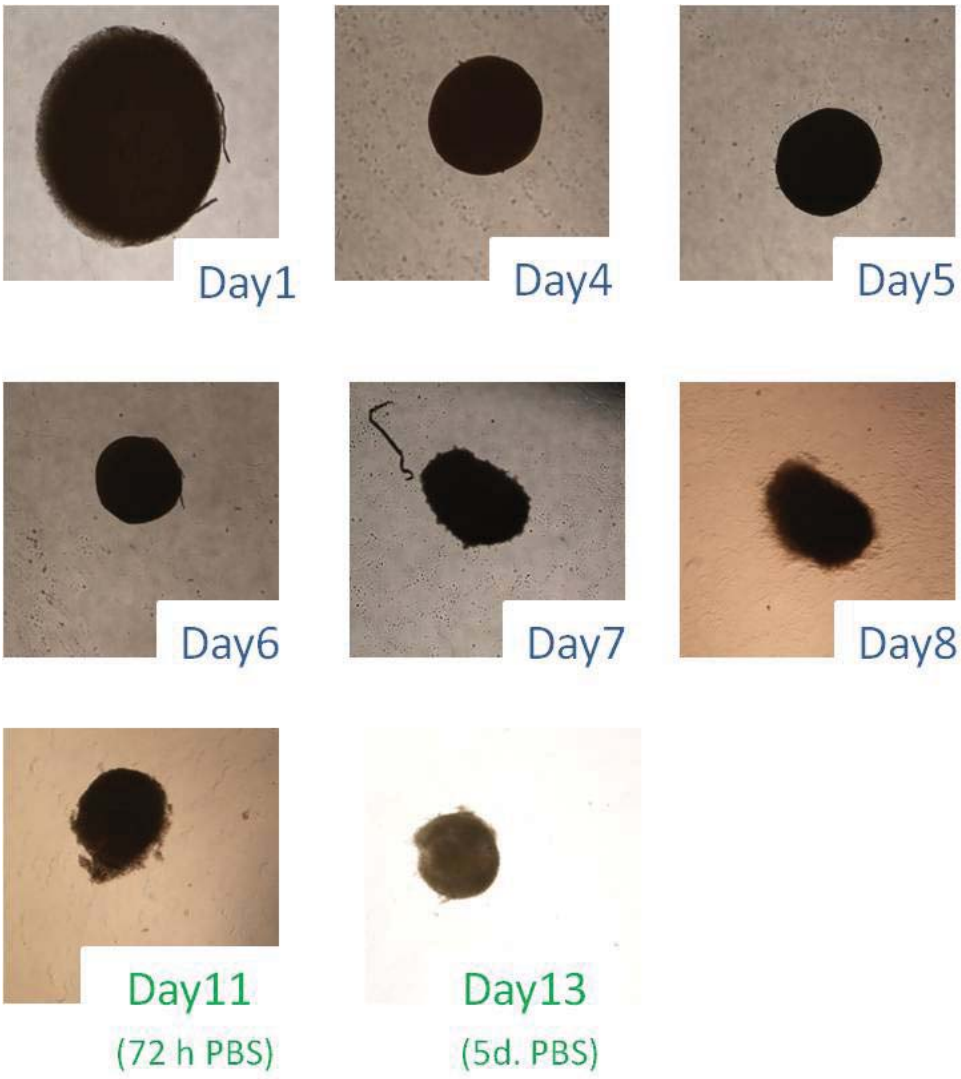

Figure 4.2: *Experimental deformation process suffer by the hydrogel after 8 days of cells in culture. In day 8 cells are killed and no reduction of the hydrogel diameter is observed in days 11 and 13 respectively.*

and Lamke 1984). At the same time, a large amount of water is squeezed from the hydrogel (Liao, Zhang et al. 2009). Both phenomena generate a previous phase of instability with cells not anchored to the substratum. Therefore in the computational model presented, this phase was not taken into consideration and the first simulation corresponded to day 1 of cell culture.

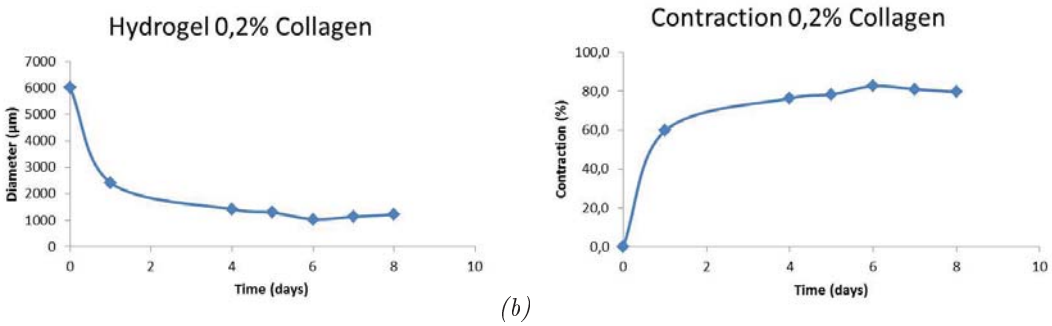

(a) *(b)*

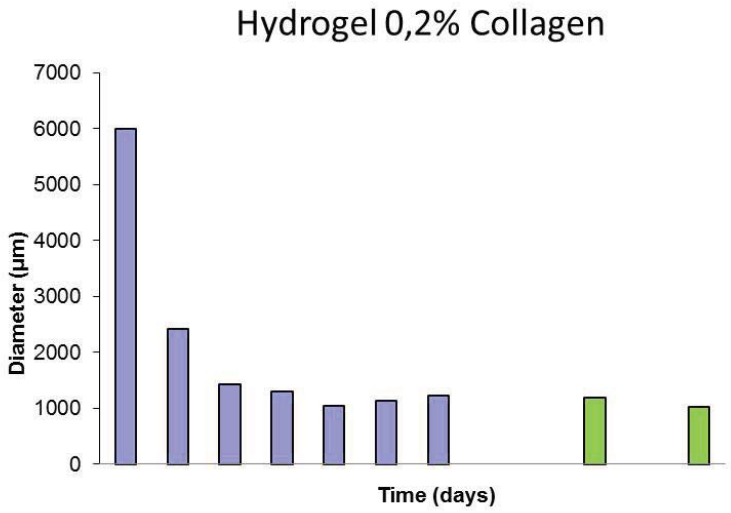

(c)

Table 4.2: *(a)Diameter reduction during 8 days of cells in culture. (b)Contraction of the hydrogel (%) during 8 days of cells in culture. (c)Blue slashs present the reduction of the hydrogel diameter during 8 days of cells in culture and green show the diameter of gels after killing cells.*

4.3.1.2 Case B. Hydrogel deformation with cells

Hydrogel properties

Collagen hydrogels 0.3% *w/v* were prepared to achieve a final thickness of 2 *mm* and 9 *mm* diameter, $1.0{\cdot}10^3$ $cells/mm^3$ were added. Table 4.3 shows the specific parameters used to reproduce this experiment (total number *n=10*).

Parameter	Description	Value	Units
n_o	Initial fibroblast concentration in the hydrogel	$1.0{\cdot}10^3$	$cells/mm^3$
Ø	Initial diameter of the hydrogel	9.0	*mm*
e	Initial thickness of the hydrogel	2.0	*mm*
ρ_{ECM}	Collagen concentration in the ECM	0.003	mg/mm^3
K	Stiffness moduli of the collagen hydrogel	$77.26{\cdot}10^{-6}$	*MPa*
v	Viscosity of the hydrogel	0.3	

Table 4.3: *Main experimental parameters selected to the collagen hydrogel contraction process.*

Sequence of hydrogel contraction obtained

The secuence of hydrogel deformation obtained with parameters collected in Table 4.3 is showed in Figure 4.3. Moreover, a quantification of hydrogel diameter reduction was collected in Table 4.4.

As previously specified, during the first day of incubation a phase of instability was generated due to the polymerization of collagen. From the second day of culture, hydrogels presented a progressive diminution of the diameter. In this point three groups of hydrogels were stablished to monitor the whole process of deformation. The first group (*n=3*) was left to deform from day 0 to day 9, analyzing 6 points during this period. A progressive diminution of the diameter was observed in all data points (table 4.4.e and f). In addition to the contraction process, the hydrogels started to adopt a folded form with a progressive thickening of the peripheric area, conforming a jellyfish-like structure. To further depict the evolution of this process, a second group of hydrogels were created. In this case, the cell culture was maintained for 16 days (*n=5*), stablishing 10 points of analysis during this period (table 4.4.c and d). Results showed, as in the first trial, the hydrogel folding with a sharper reduction in its diameter (over 60%) and generation of an empty cavity in the inferior surface (figure 4.3).This tendency was maintained until the latest point of the analysis. Finally, a third set of hydrogels was created (*n=2*), in order to determine the logevity and completion of the deformation process. These assays were maintained for 21 days, taking 11 control points during this phase (figure 4.3). Images evidenced, as in the previous sets, the abrupt reduction of the diameter and convex form adopted by hydrogels compared to the initial morphology. However, during the additional days of the culture no progression was observed, maintaining hydrogels the convex aspect and diameter of the second group analyzed (table 4.4.a and b).

Overall, based on the results obtained, it can be reported that cells embedded into the hydrogel first induce the contraction of the substrate, thickening the lower border of the gel

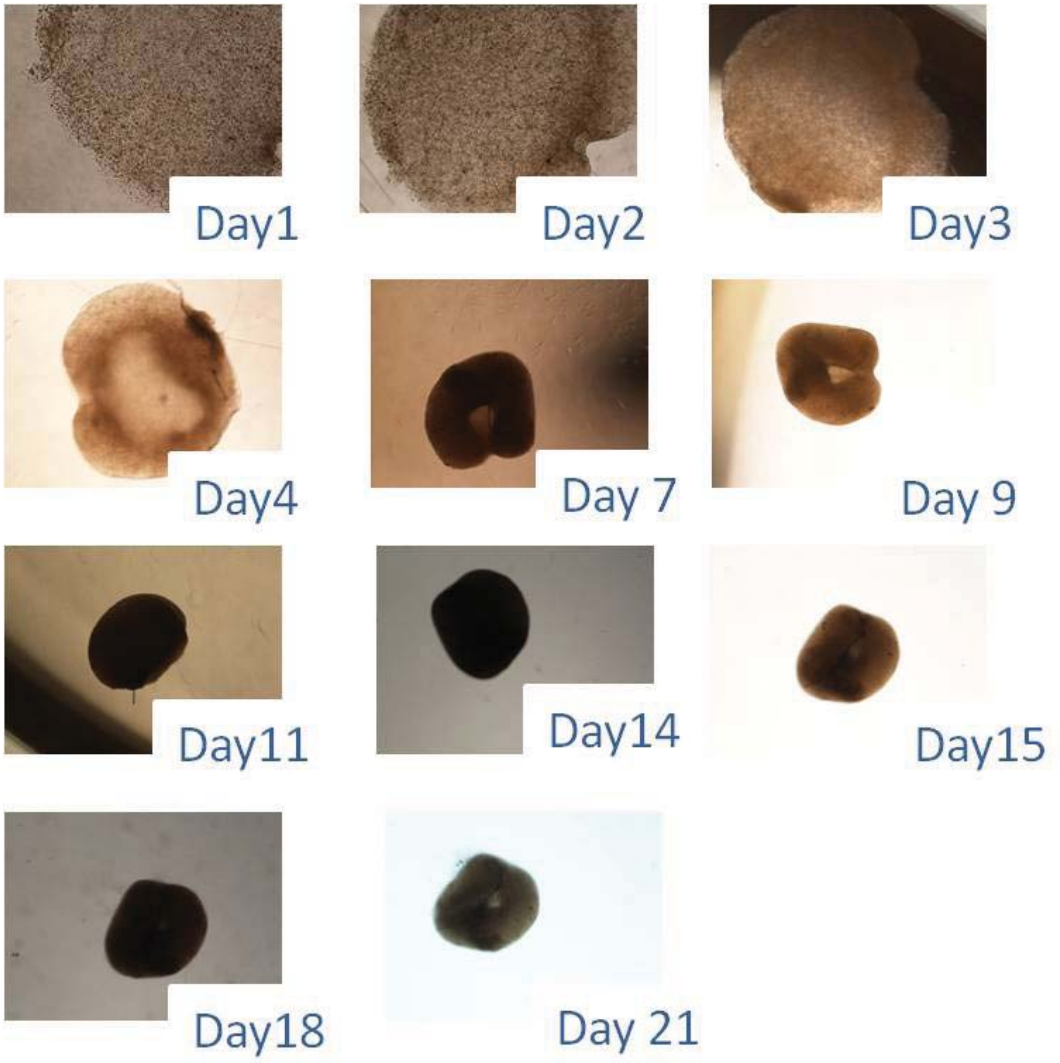

Figure 4.3: *Experimental deformation process suffer by the hydrogel after 21 days of cells in culture. In 21 days a 9 mm diameter hydrogel disk becomes compact tissue-like cell mass of approximatly 2.5 x 2.5 mm.*

and adopting the convex shape of a jellyfish. The completion of the process takes approximately 17 days, maintaining the resulting structure for at least 21 days.

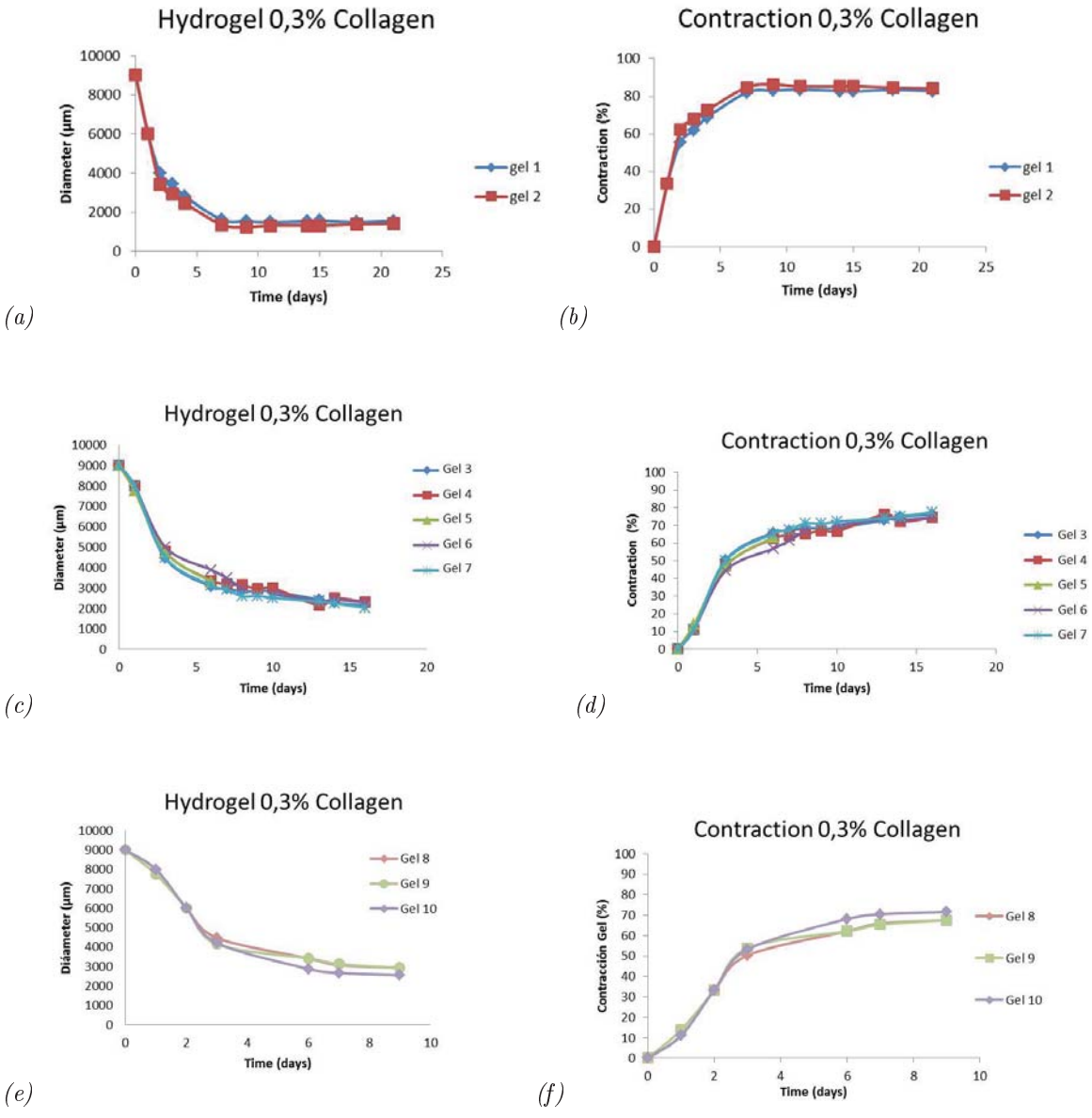

Table 4.4: Quantification of hydrogel diameter reduction and contraction. (a)Hydrogel diamter reduction during 21 days of cells in culture of two patterns. (b)Hydrogel contraction during 21 days of cells in culture of two patterns. (c)Hydrogel diameter reduction during 21 days of cells in culture of five patterns. (d)Hydrogel contraction during 16 days of cells in culture of five patterns. (e)Hydrogel diameter reduction during 9 days of cells in culture of three patterns. (f)Hydrogel contraction during 9 days of cells in culture of three patterns.

4.3.2 Morphological details

In order to confirm the experimental final shape, it was used lens 40X. Some of these pictures are collected below, and they let us to know the geometric details. Images showed in figure 4.4 reveal the morphology generated by the forces exerted by embedded fibroblasts. Top view indicates the maintenance of the "cylindrical shape". However, front view reveals the concave form that the hydrogel has adopted. In figure 4.5, the cavity formed during the process of contraction is showed.

Figure 4.4: *Top, front and bottom view respectively of the collagen hydrogel, after 21 days of cells in culture, obtained by using lens 40X.*

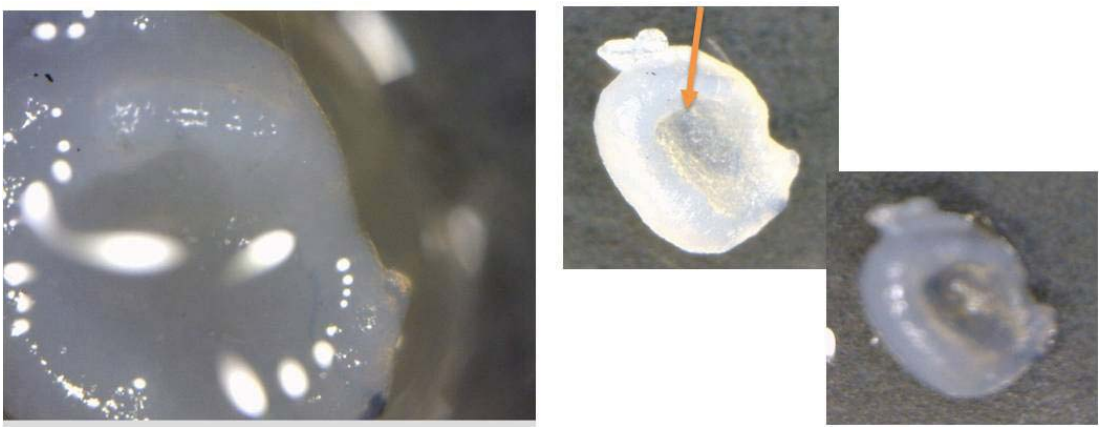

Figure 4.5: *Detail of the cavity formed in the collagen hydrogel during the contraction process. Orange arrow points to the concave area.*

Chapter 5

Model Validation: Numerical Experiments, Results and Discussion

Chapter 5 presents results obtained with simulations; it is composed of two different sections. Section 5.1 includes the morphological comparison between the hydrogel deformation obtained applying the conditions listed in the bibliography (Quintana, Muinos et al. 2009) and the bibliographic data. Section 5.2 compares results obtained by the computational model and our experimental results. In this last section, not only the morphology of the hydrogel is compared during the whole process, but also its dimensions.

5.1 Computational simulations *vs.* literature

The following results show the simulations obtained by applying the substrate rigidity indicated by Quintana et al. These simulations are mainly developed to compare the morphology of the gel during the process of contraction experienced by the substrate.

Computational parameters

	Parameter	Description	Value	Units
Initial conditions	n_o	Initial fibroblast concentration in the hydrogel	$8.0 \cdot 10^3$ $4.0 \cdot 10^3$ $1.0 \cdot 10^3$	$cells/mm^3$ $cells/mm^3$ $cells/mm^3$
Hydrogel dimensions	Ø	Initial diameter of the hydrogel	9.0	*mm*
	e	Initial thickness of the hydrogel	2.0	*mm*
Substrate parameters	ρ_{ECM}	Collagen concentration in the ECM	0.002	mg/mm^3
	K	Stiffness moduli of the collagen hydrogel	$85.0 \cdot 10^{-6}$	*MPa*
	v	Viscosity of the hydrogel	0.29	
Migration and proliferation parameters	h	Haptotaxis parameter (migration)	0.25	
	r_mitosis	Proliferation parameter	0.25	*cells/cell*

Table 5.1: *Computational paramenters coincident with Quintana´s experiment of hydrogel contraction process (Quintana, Muinos et al. 2009).*

In the course of their investigations, Quintana et al. assumed a gradual cell distribution, being the largest concentrations of cells at the bottom of the hydrogel due to gravity. In the present computational model, in agreement with this indications, a three layer cell stratification has been applied as initial cellular concentration, with 1, 4 and $8{\cdot}10^3\ cells/mm^3$ respectively from the top to the bottom of the hydrogel (table 5.1). Regarding the proliferation and migration phenomena, small values have been selected in order to simulate a smooth increment in the cell number and mobility as shown in Table 5.1.

Morphological description of the process

It is important to note that the simulation starts considering initial dimensions of 9 mm of diameter and 2 mm thickness coincident with Quintana´s experiments (Figure 5.1.c). During this first step, polymerization and water squeeze of the hydrogel induces a sharp reduction of the diameter, this phenomenon is not related to cell content and therefore was not considered into the simulation. This reduction is represented in the experimental image of the hydrogel with black arrows (Figure 5.1.c.1). Subsequently, the present model shows the contraction of the lower area of the hydrogel whereas the rest of the substrate maintains its morphology, generating an incipient convex aspect (Figure 5.1.a.2 and b.2). The evolution of this tendency with contraction of the lower area ends into a jellyfish-like structure with the thickening of the low surrounding border (Figure 5.1.a.3 and b.3); the computational simulation clearly reproduces the aspect of the hydrogel in this step (Figure 5.1.c.2). The last two steps of the simulation represent the folding of the substrate with the generation of a central empty cavity (Figure 5.1.a.4 and a.5; b.4 and b.5). The experimental data consulted in the bibliography corroborated our observations and clearly shows the internal cavity generated and external wide border conforming a convex structure (Figure 5.1.c.4).

Overall the obtained computational model accurately reproduces the main hallmarks of the hydrogel morphological deformation induced by embedded cells.

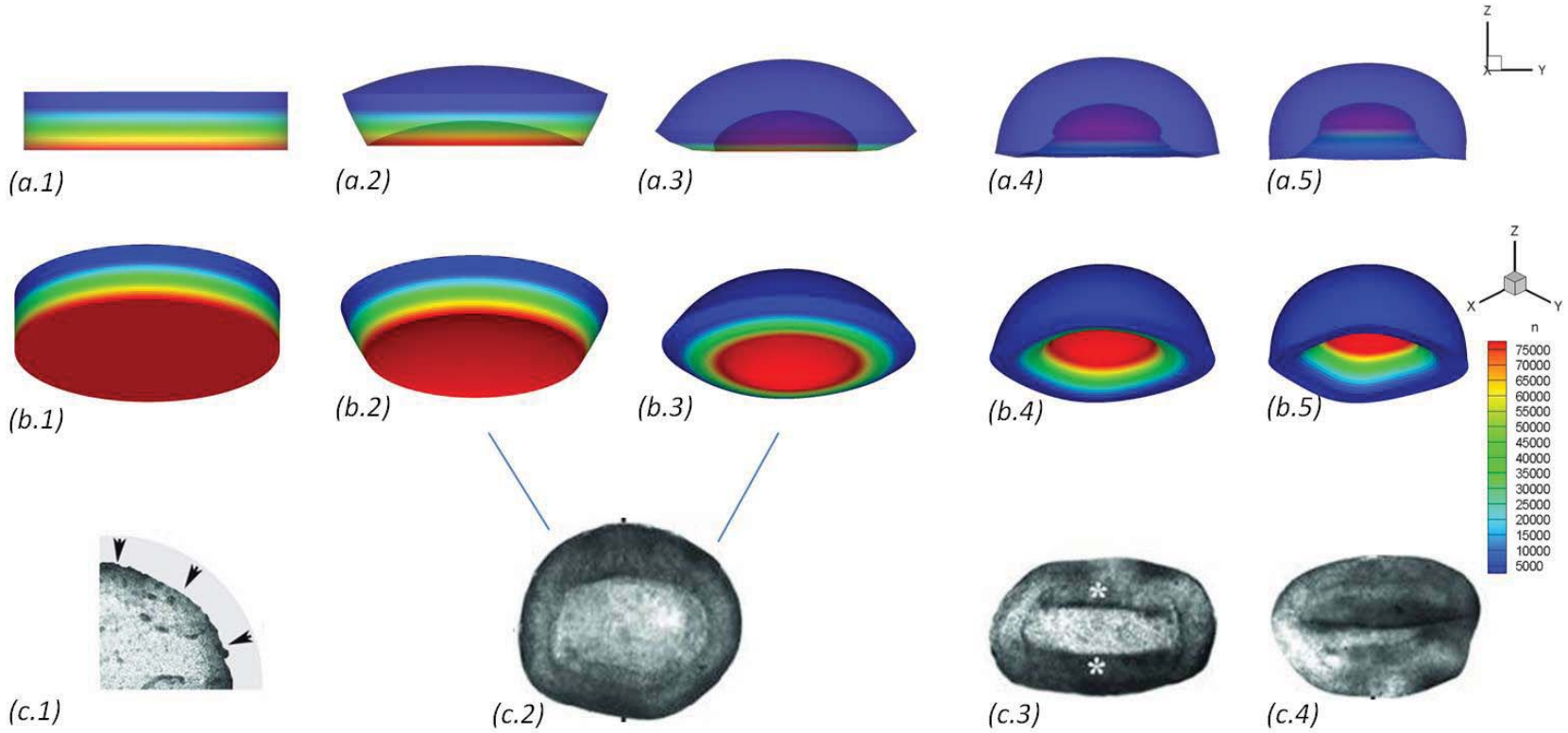

Figure 5.1: Computational simulation vs. Quintana´s experimental process. (a)Front view of simulated secuence of hydrogel contraction process. (b)Bottom view of simulated secuence of hydrogel contraction process. (c)Main morphological process observed experimentally by using confocal microscopy (Quintana, Muinos et al. 2009).

5.2 Computational simulations *vs.* our experimental data

This section comprises a description of the results obtained from the simulation of the presented computational model. In addition, a comparison of these results with the experimental data obtained for each step is included.

As above mentioned, simulation of the experimental data started 1 day postplating, due to the instability of hydrogel during polymerization process, with a homogeneous cellular distribution and the phenomenon of squeeze. The parameters selected for the simulation are shown in table 5.2.

Computational parameters

	Parameter	Description	Value	Units
Initial conditions	n_o	Initial fibroblast concentration in the hydrogel	$8.0 \cdot 10^3$ $4.0 \cdot 10^3$ $1.0 \cdot 10^3$	*cells/mm³* *cells/mm³* *cells/mm³*
Hydrogel dimensions	Ø	Initial diameter of the hydrogel	6.0	*mm*
	e	Initial thickness of the hydrogel	1.5	*mm*
Substrate parameters	ρ_{ECM}	Collagen concentration in the ECM	0.003	*mg/mm³*
	K	Stiffness moduli of the collagen hydrogel	$77{,}26 \cdot 10^{-6}$	*MPa*
	v	Viscosity of the hydrogel	0.3	
Migration and proliferation parameters	h	Haptotaxis parameter (migration)	0.25	
	r_mitosis	Proliferation parameter	0.25	*cells/cell*

Table 5.2: *Computational parameters coincident with our experiments of hydrogel contraction process.*

5.2.1 Simulation of the first step of hydrogel deformation

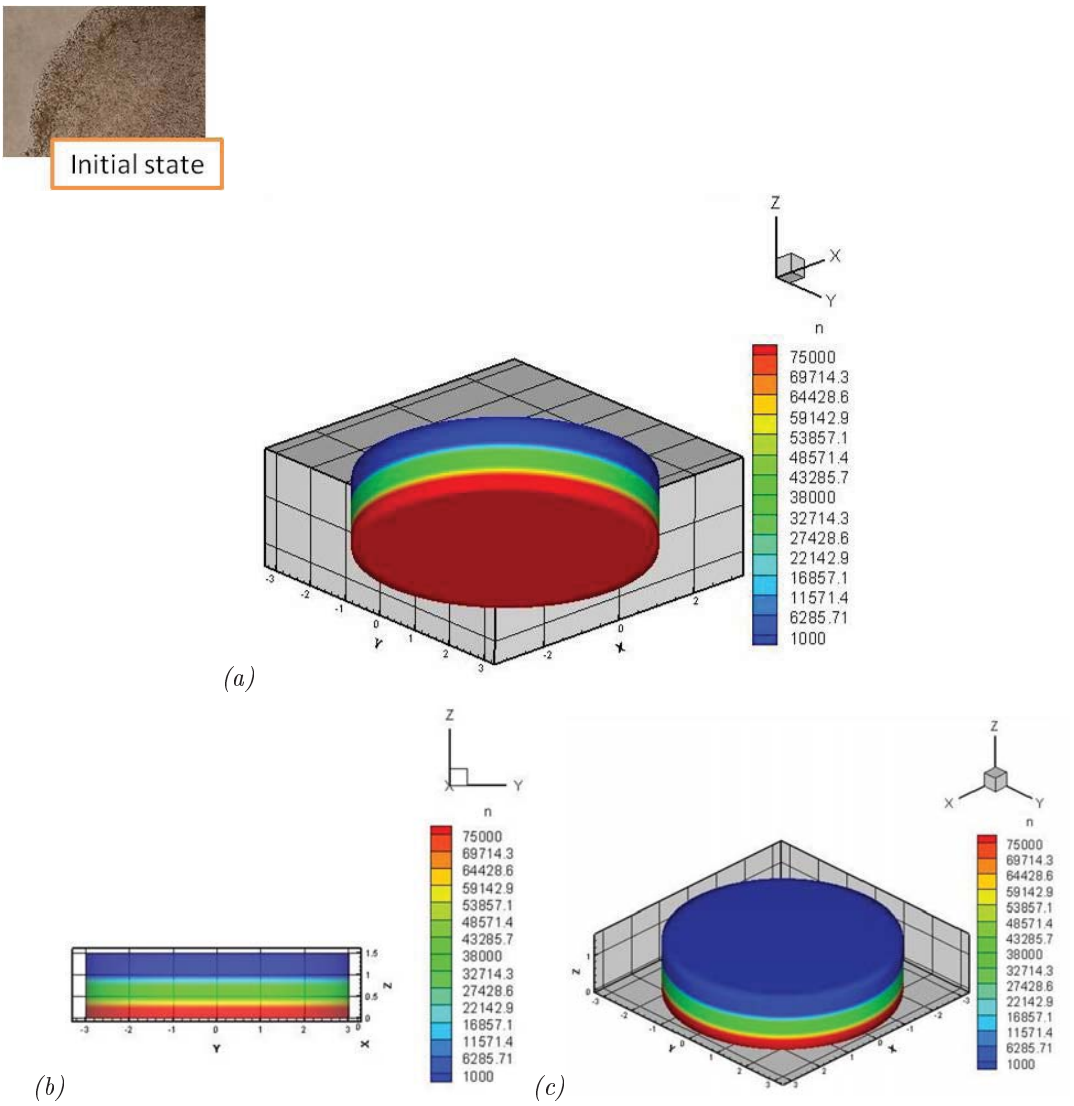

Figure 5.2: *Simulation of hydrogel contraction at the beginning of the experiment with cellular concentration (n) indicates in the legent at right. (a)Bottom view of the . (b)Front view of the hydrogel. (c)Upper view of the hydrogel.*

During the first step of the process, the proposed computational model shows the reduction of the hydrogel diameter, from 6 *mm* to the final 5.8 *mm* (Figure 5.2). Morphologically, the substrate maintains its structure of compact disk. In the other hand, the stratification of the cell concentration is observed, with higher values at the bottom of the hydrogel (approximately 80.000 $cells/mm^3$) and lower concentrations in the upper surface (1.000 $cells/mm^3$) as it is showed in the legend placed in the left of the simulations. This collected the cellular concentration (n) (Figure 5.2). This last phenomenon is considered as a consequence of the gravity.

Experimental data corroborate the presented results and figure 5.1 above shows the aspect

of the hydrogel cell culture during this first step.

5.2.2 Simulation of the second step of hydrogel deformation

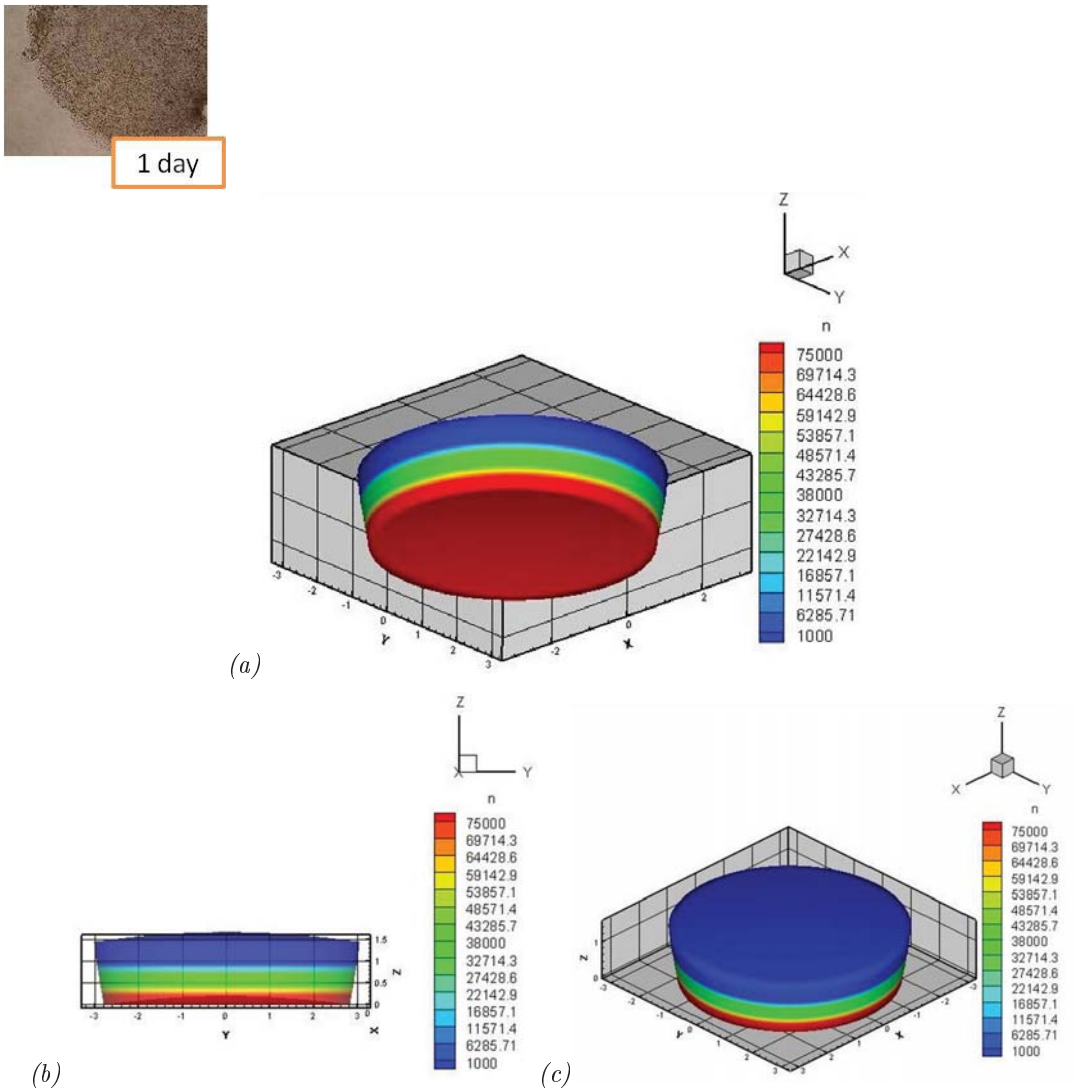

Figure 5.3: *Simulation of hydrogel contraction after 1 days of cells in cuture with cellular concentration (n) indicates in the legent at right. (a)Bottom view of the . (b)Front view of the hydrogel. (c)Upper view of the hydrogel.*

The simulation of the second step of hydrogel deformation showed the curvature of the substrate. Hydrogel became slightly convex, reducing its inner diameter to 5.6 *mm*. Cellular concentrations maintained the three layer distribution of the first step as can be appreciated in figure 5.3. The higher concentrations of the lower surface of the disk generate an elevated cellular stress in this area, as mentioned in our previous works (Manzano, Doweidar et al. 2010) that results in the substrate deformation. The experimental results confirm our simulation and image above shows the starting of the convex forming of the hydrogel.

5.2.3 Simulation of the third step of hydrogel deformation

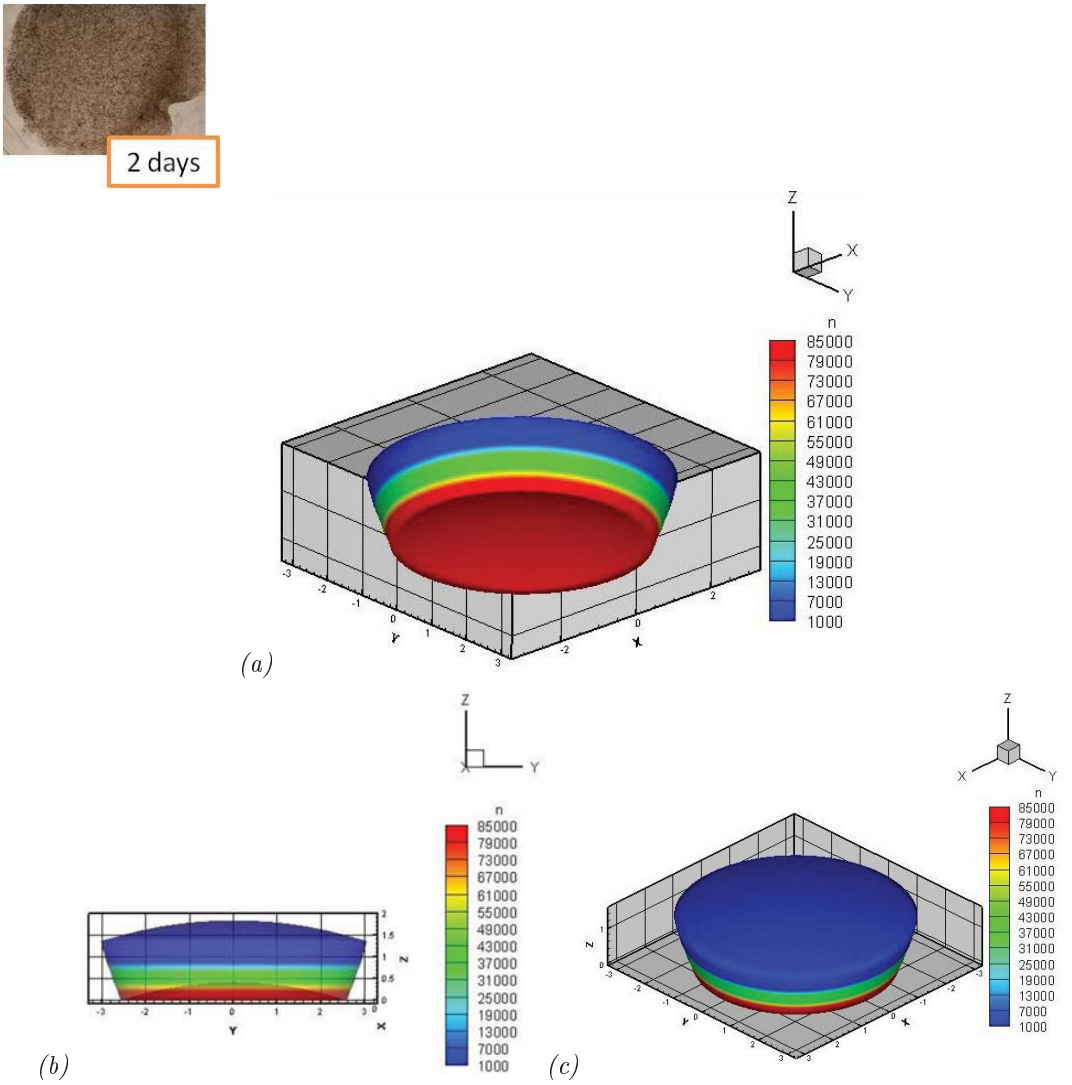

Figure 5.4: *Simulation of hydrogel contraction after 2 days of cells in cuture with cellular concentration (n) indicates in the legent at right. (a)Bottom view of the . (b)Front view of the hydrogel. (c)Upper view of the hydrogel.*

Based on bibliographic data, at this point, cell cultures reach their main proliferative potential and acquire the migration capacity (Quintana, Muinos et al. 2009). Hence, these 2 new parameters were incorporated to the present computational model as mentioned in the 3.3 section of the mathematical formulation. Importantly, proliferation has been described to be more prominent in the areas of higher cellular concentration, that in the present model correspond to the lower surface of the hydrogel. This contributes to the increment of cell concentration, and therefore, stress, in this area. In the other hand, cell migration is known to be directed to areas of higher adhesiveness (Murray, Oster et al. 1983), which are coincident with more density of the substrate (see section 3.3). In the present model, these areas correspond to

the central part of the hydrogel, which would create an hypothetical influx of cells towards this zone. However, the effect of proliferation is far more influent than migration and the balance of both parameters results in a higher concentration and cellular stress in the lower surface of the hydrogel (Figure 5.4).

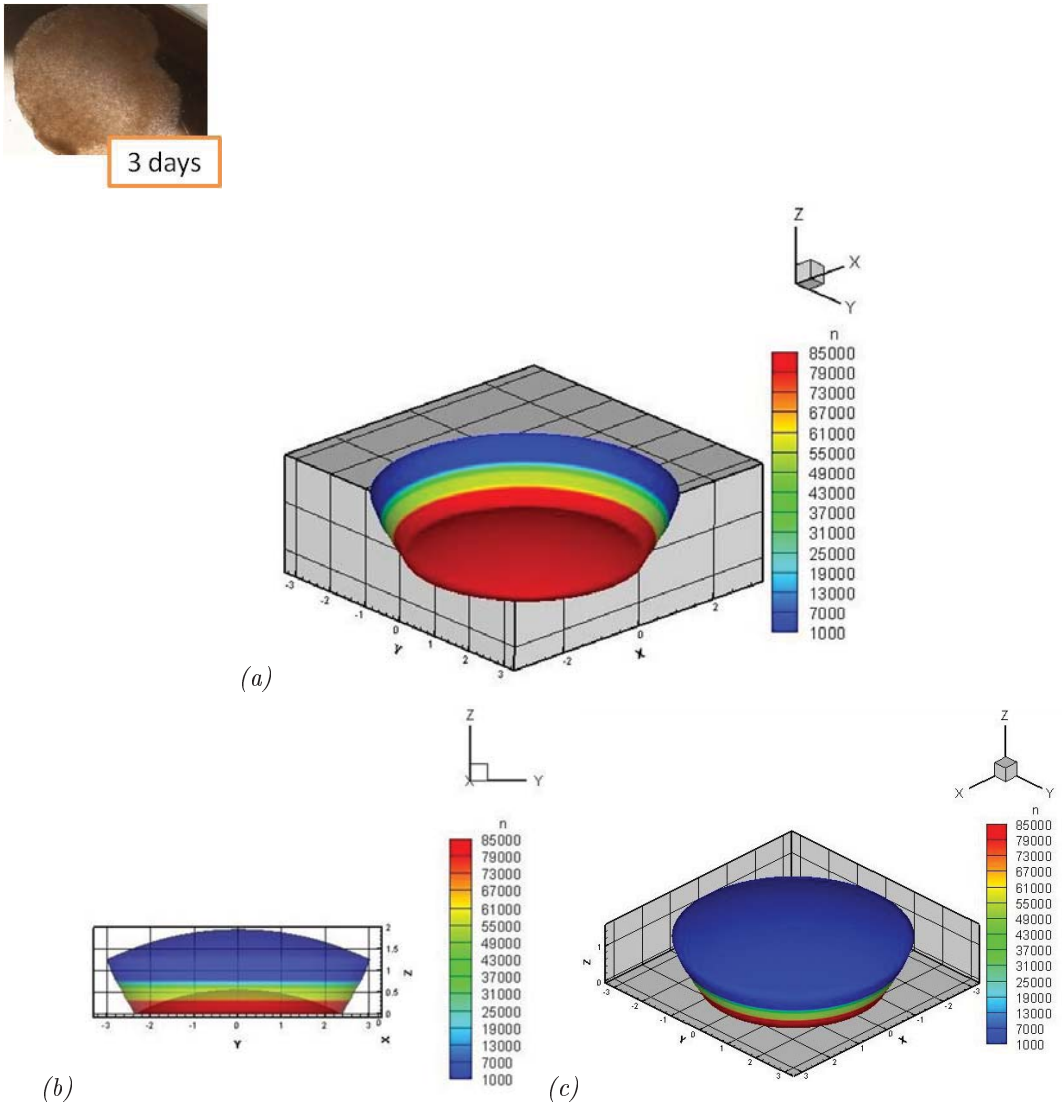

Figure 5.5: *Simulation of hydrogel contraction after 3 days of cells in cuture with cellular concentration (n) indicates in the legent at right. (a)Bottom view of the . (b)Front view of the hydrogel. (c)Upper view of the hydrogel.*

Overall, in the subsequent steps, the inclusion of these two phenomena enabled simulation to reproduce the experimental observations, and morphological changes showed the evolution of the tendency started in the last step, adopting hydrogel a progressively sharper convex aspect, with 5.2, 4.8 and 4 mm of inner diameter respectively (Figures 5.5 and 5.6).

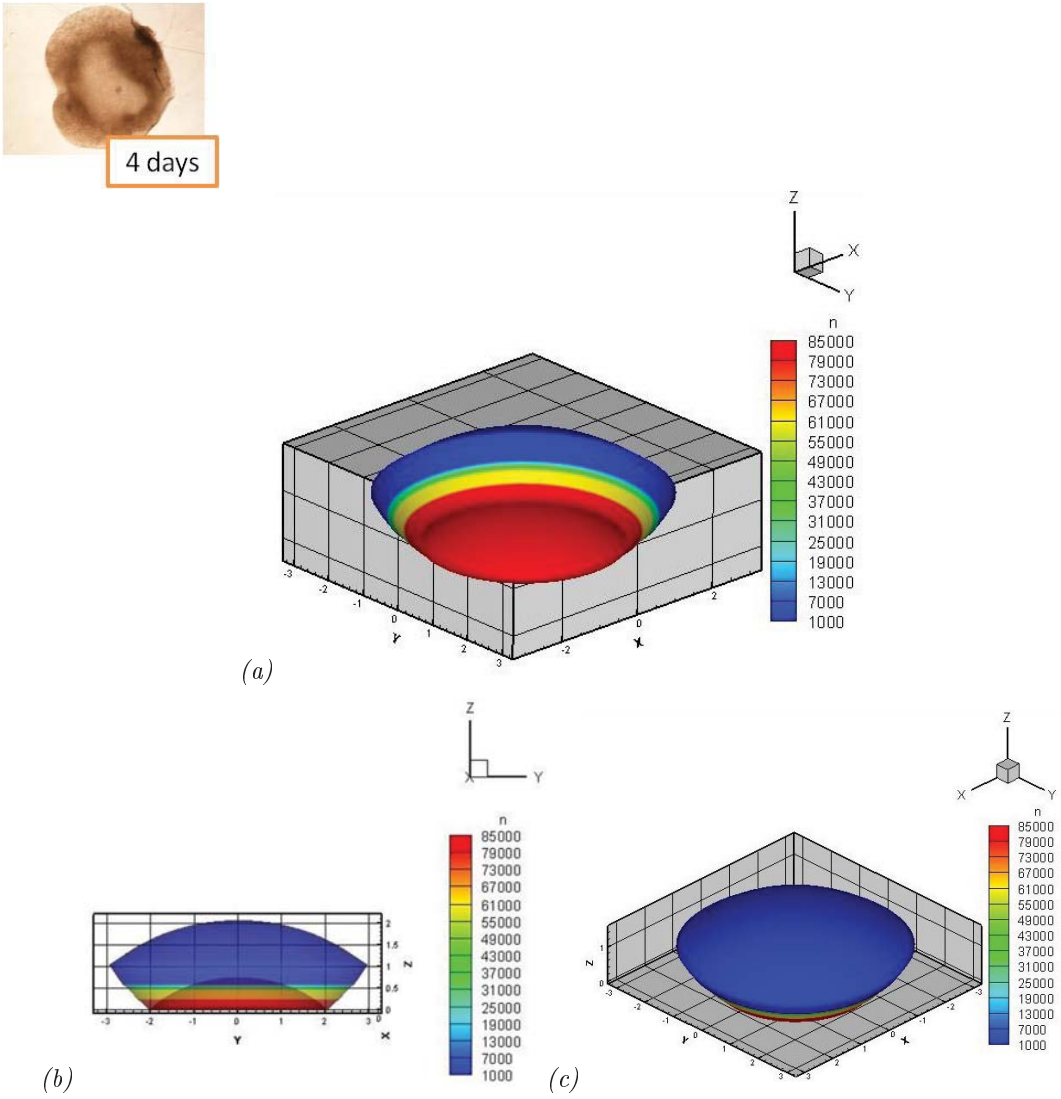

Figure 5.6: *Simulation of hydrogel contraction after 4 days of cells in cuture with cellular concentration (n) indicates in the legent at right. (a)Bottom view of the . (b)Front view of the hydrogel. (c)Upper view of the hydrogel.*

5.2.4 Simulation of the last step of hydrogel deformation

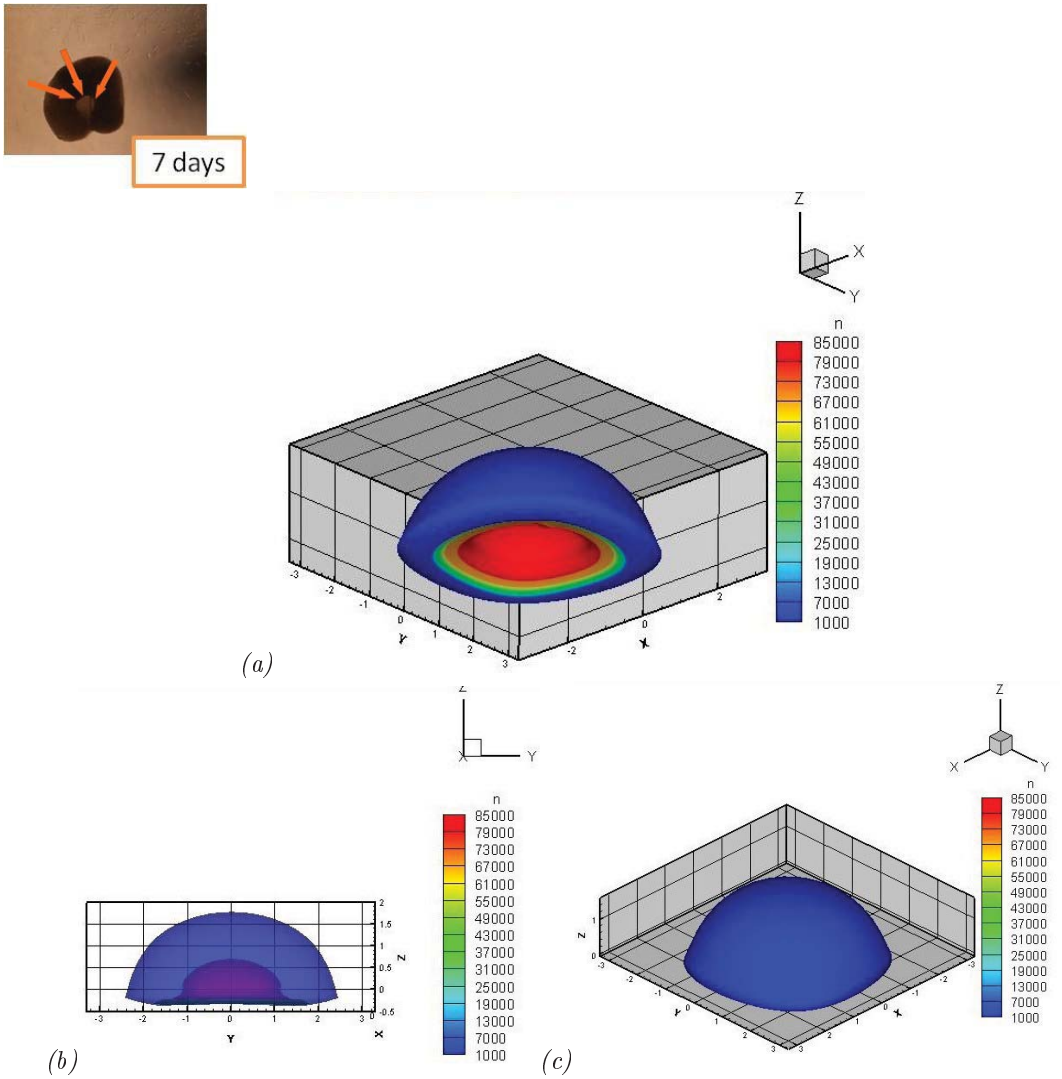

Figure 5.7: *Simulation of hydrogel contraction after 7 days of cells in cuture with cellular concentration (n) indicates in the legent at right and orange arrow shows the cavity obtained experimentally. (a)Bottom view of the . (b)Front view of the hydrogel. (c)Upper view of the hydrogel.*

During the last step of the simulation, the model shows an hydrogel with a more folded structure, due to the thickening of the lower border area and creation of an empty cavity in the center. The diameter of the internal border is reduced to 2.4 *mm* (Figure 5.7). These observations are in agreement with the experimental data obtained, where the creation of the cavity can be appreciated as a light central zone. The thickening area is observed as a round shape border in detail above and signaled with orange arrows. As in the previous steps, the stratified cellular distribution is kept, with higher concentrations in the lower areas, which based on the described arguments, would induce the folding of the hydrogel.

Table 5.3 represents the measurement of the hydrogel diameter along the 21 days of the experiment. A progressive reduction of this parameter is observed in the simulations showed above, and corresponds to the increment of the contraction. Table 5.3 represents the progressive contraction and folding of the hydrogel obtained from the proposed computational model. As can be appreciated from the comparison of both graphics, there is a clear tendency to the reduction of the substrate dimensions over the time.

Both simulation and experimental graphics, differ in the exact values of the contraction, being more prominent the reduction of the experimental hydrogel than the simulated material. However, our preliminary data and bibliography suggest that the stiffness of the substrate applied to the model strongly influences its capacity and resistance to the deformation, and therefore a candidate to explain these differences. The adjustment between experimental and simulation stiffness is currently being one of our main efforts to improve the present computational model.

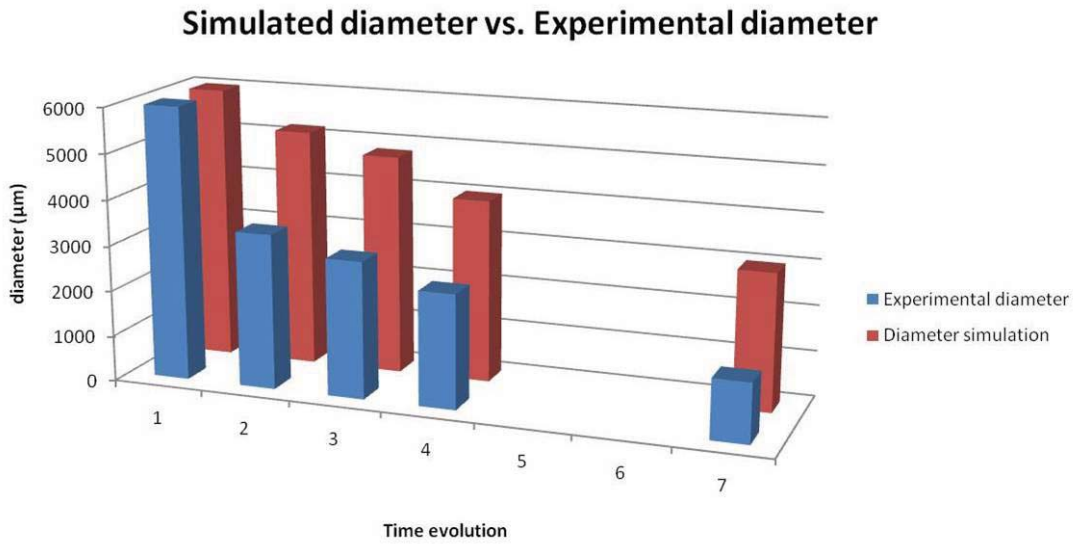

Table 5.3: *Hydrogel contraction process over the different points of measurement. Comparison between diamter of hydrogel obtained with the computational model and experimental results.*

Chapter 6

Conclusions and Future Work

6.1 Conclusions

Here I have presented an improved mechanosensing model able to explain numerous important experimental observations reported for cell-substrate interaction. This model not only has the capability of simulating the contraction process of hydrogel due to mechanical interaction cell-substrate and associates cell-generated traction forces, substrate deformation and cellular concentration but also, the migration and proliferation of cells embedded in the hydrogel.

The presented numerical model was supported by experimental work. Agreement between experimental results and simulations suggest that only considering the role of these three phenomena acting together the experimental events can be capture accurately. Moreover, the model evidences the importance of mechanical factors on cell behavior as well as the consideration of the collagen hydrogel as a vicoelastoplastic material. The model has helped us to better understand what occurs mechanically and biologically during the process and could be useful in future studies of other biological structures formation, where basic assumptions as outline in this model are coincident, as in vasculogenesis and angiogenesis. On the other hand, the presented model lacks the consideration of the phenomena related to great expulsion of water from the hydrogel and polymerization of the collagen hydrogel to capture the behavior of the gel contraction at its initial steps.

6.2 Future work

Experiences gained during the realization of this project left the door open for many future lines, below there are some,

- Firstly, in order to simulate the unstable phase that occurs before the contraction process developed in this work, it is necessary to incorporate the phenomena of squeezing water inside the hydrogel as well as the fiber reorganization due to polymerization of collagen.
- In the near future, is expected to include chemical aspects in the model. It is known that these aspects affect in the behavior of cell and even induce them to differenciate.

Bibliography

Abaqus documentation. http://www.abaqusdoc.ca/v6.8

Bell, E., B. Ivarsson, et al. (1979). "Production of a tissue-like structure by contraction of collagen lattices by human fibroblasts of different proliferative potential in vitro." Proc Natl Acad Sci U S A 76(3): 1274-8.

DiMilla, P. A., K. Barbee, et al. (1991). "Mathematical model for the effects of adhesion and mechanics on cell migration speed." Biophys J 60(1): 15-37.

Discher, D. E., P. Janmey, et al. (2005). "Tissue cells feel and respond to the stiffness of their substrate." Science 310(5751): 1139-43.

Even-Ram, S. and K. M. Yamada (2005). "Cell migration in 3D matrix." Curr Opin Cell Biol 17(5): 524-32.

Ferrenq, I., L. Tranqui, et al. (1997). "Modelling biological gel contraction by cells: mechanocellular formulation and cell traction force quantification." Acta Biotheor 45(3-4): 267-93.

Ghosh, Z. Pan, et al. (2007). "Cell adaptation to a physiologycal relevant ecm mimic with different viscoelastic properties." Biomaterials(28): 671-679.

Grinnell, F. and C. R. Lamke (1984). "Reorganization of hydrated collagen lattices by human skin fibroblasts." J Cell Sci 66: 51-63.

Guidry, C. and F. Grinnell (1985). "Studies on the mechanism of hydrated collagen gel reorganization by human skin fibroblasts." J Cell Sci 79: 67-81.

Hadjipanayi, E., V. Mudera, et al. (2009). "Guiding cell migration in 3D: a collagen matrix with graded directional stiffness." Cell Motil Cytoskeleton 66(3): 121-8.

Hawkins, R. J., M. Piel, et al. (2009). "Pushing off the walls: a mechanism of cell motility in confinement." Phys Rev Lett 102(5): 058103.

Holmes, M. J. and B. D. Sleeman (2000). "A mathematical model of tumour angiogenesis incorporating cellular traction and viscoelastic effects." J Theor Biol 202(2): 95-112.

Hughes, T. J. R. (1987). "The Finite Element Method: Linear Static and Dynamic Finite Element Analysis." Prentice-hall. Englewood Cliffs, NJ.

Liao, H., H. Zhang, et al. (2009). "Differential physical, rheological, and biological properties of rapid in situ gelable hydrogels composed of oxidized alginate and gelatin derived from marine or porcine sources." J Mater Sci Mater Med 20(6): 1263-71.

Manoussaki, D., S. R. Lubkin, et al. (1996). "A mechanical model for the formation of vascular networks in vitro." Acta Biotheor 44(3-4): 271-82.

Manzano, S., M.H. Doweidar, et al. (2010). "3D modeling of gel contraction by embedded cells."Reports Internos i3A: BIO-001-10-ART.

Moreo, P., J. M. Garcia-Aznar, et al. (2008). "Modeling mechanosensing and its effect on the migration and proliferation of adherent cells." Acta Biomater 4(3): 613-21.

Murray, J. D. (2003). "On the mechanochemical theory of biological pattern formation with application to vasculogenesis." C R Biol 326(2): 239-52.

Murray, J. D., G. F. Oster, et al. (1983). "A mechanical model for mesenchymal morphogenesis." J Math Biol 17(1): 125-9. Oster, G. F., J. D.

Murray, et al. (1983). "Mechanical aspects of mesenchymal morphogenesis." J Embryol Exp Morphol 78: 83-125. Painter, K. J. and J. A. Sherratt (2003). "Modelling the movement of interacting cell populations." J Theor Biol 225(3): 327-39.

Oster, G. F., J. D. Murray, et al. (1983). "Mechanical aspects of mesenchymal morphogenesis." J Embryol Exp Morphol 78: 83-125. Painter, K. J. and J. A. Sherratt (2003). "Modelling the movement of interacting cell populations." J Theor Biol 225(3): 327-39.

Painter, K. J. and J. A. Sherratt (2003). "Modelling the movement of interacting cell populations." J Theor Biol 225(3): 327-39.

Quintana, L., T. F. Muinos, et al. (2009). "Early tissue patterning recreated by mouse embryonic fibroblasts in a three-dimensional environment." Tissue Eng Part A 15(1): 45-54.

Ramtani, S. (2004). "Mechanical modelling of cell/ECM and cell/cell interactions during the contraction of a fibroblast-populated collagen microsphere: theory and model simulation." J Biomech 37(11): 1709-18.

Rangarajan, R. and M. H. Zaman (2008). "Modeling cell migration in 3D: Status and challenges." Cell Adh Migr 2(2): 106-9.

Réseau Québécois de calcul de haute performance (2011). http://public.rqchp.ca/

Tingstrom, A., C. H. Heldin, et al. (1992). "Regulation of fibroblast-mediated collagen gel contraction by platelet-derived growth factor, interleukin-1 alpha and transforming growth factor-beta 1." J Cell Sci 102 (Pt 2): 315-22.

Zahm, J. M., H. Kaplan, et al. (1997). "Cell migration and proliferation during the in vitro wound repair of the respiratory epithelium." Cell Motil Cytoskeleton 37(1): 33-43.

Zaman, M. H., R. D. Kamm, et al. (2005). "Computational model for cell migration in three-dimensional matrices." Biophys J 89(2): 1389-97.

Zaman, M. H., L. M. Trapani, et al. (2006). "Migration of tumor cells in 3D matrices is governed by matrix stiffness along with cell-matrix adhesion and proteolysis." Proc Natl Acad Sci U S A 103(29): 10889-94.